

UC Irvine

UC Irvine Electronic Theses and Dissertations

Title

Single Molecule Rotational Inelastic Electron Tunneling Spectroscopy and Microscopy

Permalink

<https://escholarship.org/uc/item/38t6r9kb>

Author

Li, Shaowei

Publication Date

2015

Peer reviewed|Thesis/dissertation

UNIVERSITY OF CALIFORNIA,
IRVINE

Single Molecule Rotational Inelastic Electron Tunneling Spectroscopy and Microscopy

THESIS

submitted in partial satisfaction of the requirements
for the degree of

MASTER OF SCIENCE

in Physics

by

Shaowei Li

Dissertation Committee:
Professor Wilson Ho, Chair
Professor Steven White
Professor Jing Xia

2015

Portion of Chapter 2 © 2013 American Physical Society
Portion of Chapter 3 © 2015 American Physical Society
All other materials © 2015 Shaowei Li

DEDICATION

To

my wife, Jieyun

my parents

TABLE OF CONTENTS

	Page
LIST OF FIGURES	v
LIST OF TABLES	vi
ACKNOWLEDGMENTS	vii
CURRICULUM VITAE	ix
ABSTRACT OF THE DISSERTATION	xiii
CHAPTER 1: Introduction	1
1.1 Background and Motivation	1
1.2 Bibliography	4
CHAPTER 2: Rotational and Vibrational Excitations of a Hydrogen Molecule Trapped within a Nanocavity of Tunable Dimension	5
2.1 Abstract	5
2.2 Introduction	5
2.3 Methods	7
2.4 Results and Discussion	8
2.5 Conclusion	17
2.6 Bibliography	20
CHAPTER 3: Rotational Spectromicroscopy: Imaging the Orbital Interaction between Molecular Hydrogen and an Adsorbed Molecule	22
3.1 Abstract	22
3.2 Introduction	22
3.3 Methods	24

3.4 Results and Discussion	25
3.5 Conclusion	43
3.6 Bibliography	51
CHAPTER 4: Conclusions and Prospects	53
4.1 Concluding Remarks	53
4.2 Prospects for the Future	53
4.3 Bibliography	54

LIST OF FIGURES

		Page
Figure 1.1	Schematic diagram of the inelastic tunneling process.	3
Figure 2.1	A hydrogen molecule trapped in the tunneling junction of STM.	10
Figure 2.2	Tunneling spectra taken before and after dosing molecular hydrogen or its isotopes.	13
Figure 2.3	IETS at different tip-substrate separations.	16
Figure 2.4	DFT calculations.	19
Figure 3.1	Reversible electron transfer to a single MgP molecule interacting with H ₂ in a double barrier tunnel junction of the STM.	27
Figure 3.2	Rotational spectra of single H ₂ molecule interacting locally with Mg-porphyrin measured by STM-IETS.	30
Figure 3.3	Single molecule rotational imaging.	33
Figure 3.4	MgP over NiAl surface.	36
Figure 3.5	IETS measurements of trapped H ₂ at different tip-substrate separations.	39
Figure 3.6	Calculated partial density of states under different conditions.	42
Figure 3.4	DFT result of H ₂ adsorption energies at different positions over MgP	45

LIST OF TABLES

		Page
Table 3.1	DFT results of H ₂ adsorption energies at different positions over MgP.	48

ACKNOWLEDGMENTS

Foremost, I would like to express the deepest appreciation to my advisor, Professor Wilson Ho, who provides me the guidance and financial support to pursuit the research presented in this thesis. I have been given both academic freedom and scientific instructions and benefited greatly from his passion for science and extremely high standard of excellence.

I would like to thank Professor Steven White and Professor Jing Xia for serving as my dissertation committee, and Professor Ruqian Wu and Professor Nien-Hui Ge as my advancement committee.

Special thanks to the group members who run experiments with me: Arthur Yu, for his dedication for almost every projects presented in this thesis; Dr. Freddy Toledo and Zhumin Han, for their support in revealing the rotational mode of a single molecule; Greg Czap, for his help in visualizing the intermolecular interaction.

I would also like to thank my collaborators in Professor Ruqian Wu's group: Dr. Hui Wang, Dr. Haiyan He, and Dr. Dingwang Yuan for the theoretical calculations which provide deep insight to our experimental observations.

During my time in Ho group, I have always been enjoying working with other members: Dr. Qing Huan, Dr. Ying Jiang, Dr. Ungdon Ham and Dr. Chilun Jiang who guided me how to operate the apparatus during my first two years; Dr. Hikari Kimura, Dr. Weicai Cao and Calvin Patel, for their valuable help in operating the laser systems; Dr. Haigang Zhang, Chen Xu and HanKyu Lee for their efforts in the instrumentation projects; Siyu Chen, Jiang Yao, Likun Wang, Peter Wagner, Christian Kim for their help and friendship. It is a pleasure to work with all of you in Ho group.

Finally, I would like to thank National Science Foundation Center for Chemical Innovation on Chemistry at the Space-Time Limit (CaSTL) under Grant No. CHE-0802913 and Chemical Science, Geo- and Bioscience Division, Office of Science, U.S. Department of Energy, under Grant No. DE-FG02-04ER1595 for the funding support in carrying out this research.

CURRICULUM VITAE

Shaowei Li

EDUCATION

Bachelor of Science in Physics (Honors), Department of Physics, Nankai University (06/2010)

Ph.D Candidate in Physics, Department of Physics and Astronomy, UC Irvine (03/2012)

Master of Science in Physics, Department of Physics and Astronomy, UC Irvine (12/2015)

RESEARCH EXPERIENCE

- **GRADUATE STUDENT RESEARCHER, (07/2010 -present)**

Wilson Ho Group, Department of Physics and Astronomy, UC Irvine

Inelastic Excitation of Single Molecule using Scanning Tunneling Microscope

- **UNDERGRADUATE STUDENT RESEARCHER, (07/2009 -07/2010)**

Xinghua Lu Group, Institute of Physics, Chinese Academy of Sciences

Design and Fabrication of Photo Assisted Scanning Tunneling Microscope

- **SUMMER INTERN, (07/2008-09/2008)**

Ningbo Institute of Materials Technology& Engineering, Chinese Academy of Sciences

Synthesis of metal oxide varistor material

- **PROJECT LEADER, (12/2007 -05/2009)**

Nankai University

Project Director of China's National Undergraduate Innovation Experiment Project (funded by

Ministry of Education), "Microwave Laundry Dryer"

TEACHING EXPERIENCE

- **Grader**, Undergraduate Thermal Dynamics, (09/2010-12/2010)

- **Grader**, Undergraduate Electromagnetics, (01/2011-03/2011)

- **Teaching Assistant**, Undergraduate Quantum Mechanics, (03/2011-12/2011)

- **Teaching Assistant**, Graduate Electromagnetics, (1/2011-3/2011)

- **Teaching Assistant**, Graduate Numerical Method, (1/2011-3/2011)

RESEARCH INTEREST

- **Development and application of new instrumentation and technique**
Laser-assisted Scanning Tunneling Microscope
Software programming for home-made Scanning Tunneling Microscope
- **Single-molecule physics and chemistry**
Vibrational and rotational excitation of single molecule
Control, manipulation and synthesis of single chemical bonds
Scanning Tunneling Microscope induced light emission from single molecule
- **Low-dimensional quantum materials**
Electronic and plasmonic properties of nano particles

PUBLICATIONS

- **Shaowei Li**, Arthur Yu, Freddy Toledo, Zhumin Han, Hui Wang, H. Y. He, Ruqian Wu, and W. Ho, “Rotational and Vibrational Excitations of a Hydrogen Molecule Trapped within a Nanocavity of Tunable Dimension”, **Phys. Rev. Lett.** 111, 146102 (2013)
- **Shaowei Li**, Dingwang Yuan, Arthur Yu, Gregory Czap, Ruqian Wu, W. Ho, “Rotational Spectromicroscopy: Imaging the Orbital Interaction Between Molecular Hydrogen and an Adsorbed Molecule”, **Phys. Rev. Lett.** 114, 206101 (2015)
- Arthur Yu, **Shaowei Li**, Gregory Czap, and W. Ho, “Single-Molecule Rotational and Vibrational Spectroscopy and Microscopy with the Scanning Tunneling Microscope”, **J. Phys. Chem. C.** 119, 26 (2015)
- Hui Wang, **Shaowei Li**, H. Y. He, Arthur Yu, Freddy Toledo, Zhumin Han, W. Ho, Ruqian Wu, “Trapping and Characterization of a Single Hydrogen Molecule in a Continuously Tunable Nanocavity” **J. Phys. Chem. Lett.** 6, 2453 (2015)

PATENTS

- **Shaowei Li**, Microwave Laundry Dryer , China National practical new-type patent, 200920053803.8
- Xinghua Lu, **Shaowei Li**, Shichao Yan, Xiaodong Guo, Nan Xie, Light Collection System for Scanning Tunnel Microscope, China National Invention Patent, 201010160542.7

SEMINAR AND CONFERENCE TALKS

- **Surface Physics Lecture Series**, Institute of Physics, Chinese Academy of Sciences, (12/2014)
Invited Talk: Rotational Spectromicroscopy with Scanning Tunneling Microscope
- **Physics Today Seminars**, School of Physics, Nankai University, (12/2014)
Invited Talk: Visualization of Quantum Mechanics
- **ICN+T 2014 International Conference on Nanoscience** at Vail (07/2013)
Contributed Talk: Controlling Hydrogen Dissociation by the Scanning Tunneling Microscope
Contributed Talk: Visualization of the Intermolecular Hybridization from Hydrogen Rotation
- **AVS 60th International Symposium and Exhibition** at Long Beach (10/2013)
Contributed Talk: Real-space Spectroscopy and Microscopy of Tunneling Electron Induced Light Emission from Single Gold Nanoparticle
- **APS March Meeting** at Baltimore (03/2013)
Contributed Talk: Rotational Spectroscopy at Sub-Angstrom Level: Rotational and Vibrational Excitations of Molecular Hydrogen Measured by the Scanning Tunneling Microscope
- **APS California Section Annual Meeting** at San Luis Obispo (10/2012)
Contributed Talk: Real Space Rotational Spectroscopy: Measurement of the Rotational Excitation of a Single Molecule by the Scanning Tunneling Microscope

HONORS

- **Regents' Fellowship**, UC Irvine, (07/2010)
- **China's National Scholarship** (11/2009)
- **1st Prize** of 10th "**Challenge Cup**" Tianjin's Undergraduate Curricular Academic Science and Technology Works by Race (07/2009)
- **2nd Prize as an Excellent Project** in China's National Undergraduate Innovation Experiment Project (06/2009)
- **1st Prize of Excellent Undergraduate Scholarship** of Nankai University (10/2008)

LANGUAGE

- English, Mandarin, Cantonese

PROGRAMING LANGUAGE

- C, C#, Java, LabView

ABSTRACT OF THE DISSERTATION

Single Molecule Rotational Inelastic Electron Tunneling Spectroscopy and Microscopy

By

Shaowei Li

Master of Science in Physics

University of California, Irvine, 2015

Professor Wilson Ho, Chair

The power of rotational spectroscopy has long been demonstrated in the frequency domain by microwave spectroscopy, but its application in real space has been limited. Using a scanning tunneling microscope (STM) and inelastic electron tunneling spectroscopy (IETS), we were able to conduct real-space measurements of rotational transitions of gaseous hydrogen molecules physisorbed on surfaces at 10 K. The $j=0$ to $j=2$ rotational transition for para- H_2 and HD were observed by STM-IETS. It is also found that the rotational energy is very sensitive to its local environment, we could precisely investigate how the environmental coupling modifies the structure, including the bond length, of a single molecule with sub-Angstrom resolution. Due to this high sensitivity, the spatial variation in the potential energy surface can be quantified by the rotational and vibrational energies of the trapped H_2 . The ability of the tip to drag along a hydrogen molecule as it scans over another adsorbed molecule combined with the sensitivity of the hydrogen rotational excitation recorded by IETS to its immediate environment lead to the implementation of rotational spectromicroscopy. Hydrogen rotational spectroscopy and microscopy provides novel approach toward visualizing and quantifying the intermolecular interaction as well as the intermediate processes of chemical reactions.

Chapter 1

Introduction

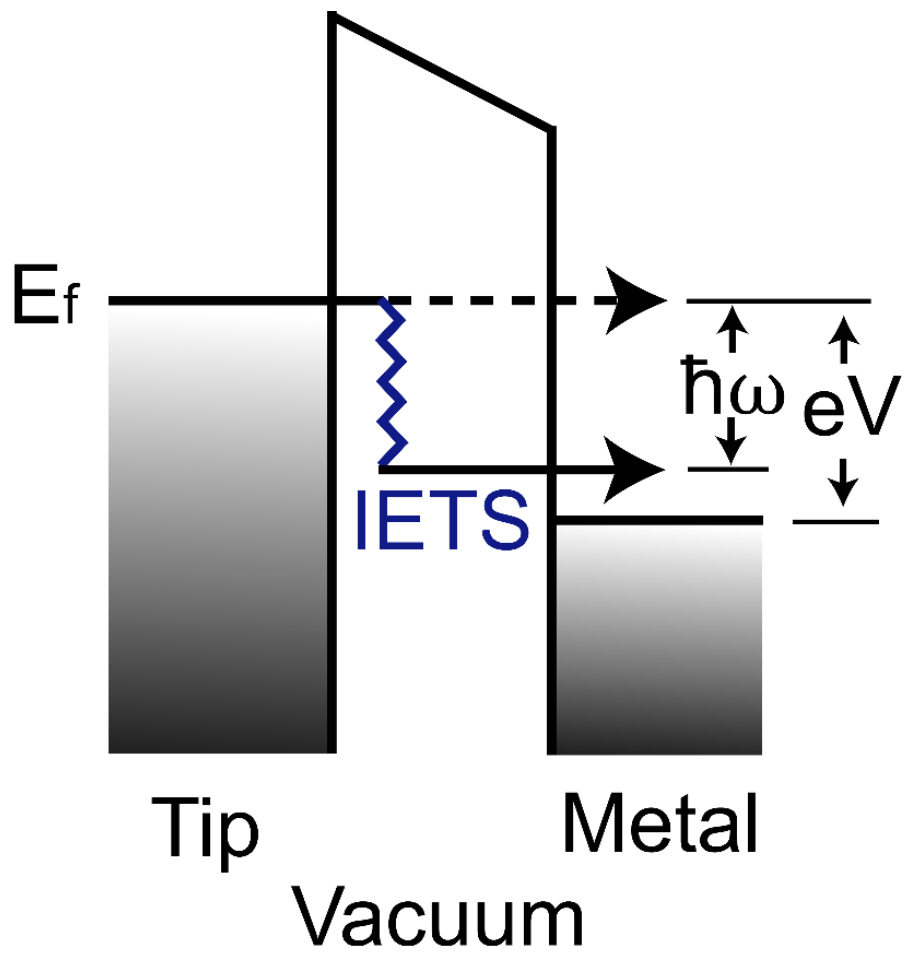
1.1 Background and Motivation

Since its invention, the unparalleled ultra-high spatial resolution made the Scanning Tunneling Microscope (STM) [1] a powerful tool to investigate the physical and chemical phenomena on surfaces. Numerous efforts have been made to expand the capabilities of STM in addition to its atomic scale spatial resolution. It has been proved that the local electronic structure can be probed from the tunneling current signal using scanning tunneling spectroscopy [2]. The STM tip can be used to manipulate atoms and molecules [3]. One important milestone is the demonstration of STM inelastic electron tunneling spectroscopy (IETS). The vibrations of single molecule on the surface can be detected in the real space [4].

As indicated in Fig. 1.1, the excitation of an inelastic excitation will open a constant conductance channel for electrons and result in a slope change in the I-V curve. A step like change can be observed in the dI/dV signal at the energy of the inelastic excitation. In the dI^2/d^2V spectra, a peak can be found at the positive bias, and a dip can be found at the negative bias. The energy of this peak (or dip) will be the excitation energy [5].

Since the first demonstration of vibrational STM-IETS, other inelastic excitations such as phonon [6] and spin flip [7] were soon reported. However, the detection rotational excitation of single molecule have met with little success because of the experimental challenges of probing a gaseous molecule on surface. In this dissertation, we will focus on the demonstration of single molecule rotational spectroscopy and microscopy using STM-IETS.

FIG. 1.1. Schematic diagram of the inelastic tunneling process.



1.2 Bibliography

- [1] G. Binnig, H. Rohrer, C. Gerber and E. Weibel, Phys. Rev. Lett. **49**, 57 (1982).
- [2] R. M. Feenstra, J. A. Stroscio and A. P. Fein, Surf. Sci. Lett. **181**, 295 (1987).
- [3] H. J. Lee and W. Ho, Science **26**, 1719 (1999).
- [4] B. C. Stipe, M. A. Rezaei and W. Ho, Science, **280**, 1732 (1998).
- [5] W. Ho, J. Chem. Phys. **117**, 11033 (2002).
- [6] Y. Zhang, V. W. Brar, F Wang, C. Girit, Y. Yayan, M. Panlasigui, A. Zettl and M. F. Crommie, Nat. Phys. **4**, 627 (2008).
- [7] A. J. Heinrich, J. A. Gupta, C. P. Lutz, and D. M. Eigler, Science **306**, 466 (2004).

Chapter 2

Rotational and Vibrational Excitations of a Hydrogen Molecule Trapped Within a Nanocavity of Tunable Dimension

2.1 Abstract

The rotational and vibrational transitions of a hydrogen molecule weakly adsorbed on the Au(110) surface at 10 K were detected by inelastic electron tunneling spectroscopy with a scanning tunneling microscope. The energies of the $j=0$ to $j=2$ rotational transition for para-H₂ and HD indicate that the molecule behaves as a three-dimensional rigid rotor trapped within the tunnel junction. An increase in the bond length of H₂ was precisely measured from the downshift in the rotational energy as the tip-substrate distance decreases.

2.2 Introduction

Rotational and vibrational transitions can reveal structural and energetic properties of molecules [1,2]. Even small changes in the distance between atoms or the masses from isotopic substitution alter the rotational and vibrational transition energies of the molecule. The power of vibrational and rotational spectroscopies has been demonstrated in the frequency [3-5] and time [6-7] domains in the infrared and microwave. The sensitivity of vibrational spectroscopy has reached the single bond level by the detection of vibrationally inelastic electron tunneling process using the scanning tunneling microscope (STM) [8]. However, the detection of rotational transitions in single molecules remains to be demonstrated.

Hydrogen, the lightest element in the universe, plays a particularly important role in the development of quantum mechanics. Exact solutions to the Schrödinger equation can be obtained for atomic and molecular hydrogen. The rotational states of the hydrogen molecule can be analyzed within the rigid rotor model. The smallest mass of hydrogen (H) and the large percent difference in mass from its isotope deuterium (D) yield high and large shift in energies for the rotational transitions that facilitate detection.

The detection of the rotational transitions of molecular hydrogen using the STM requires that the bonding between molecule and substrate should be sufficiently weak so the adsorbed molecule behaves like a gas phase molecule, but the molecule needs to be sufficiently stable for I-V, dI/dV and d^2I/dV^2 scanning tunneling spectroscopy (STS). On noble metal surfaces such as Au(110), molecular hydrogen are weakly adsorbed at low temperature via van der Waals forces [9,10]. The adsorbed molecules are mobile and can rapidly migrate one by one in and out of the tip-surface tunnel junction, on a time scale much shorter than the imaging time. [10,11]. In the tunneling range, the tip-substrate separation is 6.5 Å to 7.5 Å in our measurement. At the same time, tunneling occurs just below the tip apex, and the tunneling current is confined laterally within sub-Ångström. In such a junction, only a single hydrogen molecule can be trapped at any given time [12,13]. Although the spectroscopic signals are the average over many molecules from the diffusion and trapping processes, each trapped hydrogen molecule is experiencing the same environmental coupling given by the tip-substrate junction, and variations in the configurations and properties of different molecules are expected to be insignificant. The trapped hydrogen molecule dramatically increases the contrast of the STM topographic images, providing new details of complex surface structures [11,12]. In addition, as each trapped molecule is separated from other surrounding molecules, it maintains the essential properties as an isolated molecule that exhibits the rotational

and vibrational properties of a nearly free molecule trapped within a nanocavity of tunable dimension.

Here, we demonstrate rotational spectroscopy with the STM. In the inelastic electron tunneling spectroscopy (IETS) with the STM, excitations are characterized as step changes in the dI/dV spectrum at the threshold voltage corresponding to these excitations. The STM-IETS of H_2 , D_2 , and HD molecules weakly adsorbed on the Au(110) surface shows a series of step changes in the dI/dV spectra, which correspond to rotational and vibrational excitations. In these dI/dV spectra, $j=0 \rightarrow 2$ rotational excitations of H_2 and HD are recorded as an increase in conductance while the $\nu=0 \rightarrow 1$ vibrational excitation in the adsorption well of H_2 , D_2 , and HD shows a decrease in conductance. The coupling of the rotational motions of the hydrogen molecule to its environment given by the metallic tip and substrate is determined by squeezing the tip-substrate separation.

2.3 Methods

The experiments were performed using a home-built STM operating at 10 K and a base pressure of 3×10^{-11} Torr [14]. The Au(110) surface was cleaned by cycles of Ne^+ sputtering and annealing at 680 K. The silver tip was electrochemically etched. The clean surface at 10 K was dosed either with H_2 , HD or D_2 at 2×10^{-10} Torr for 5 min. The adsorb molecule can be completely desorbed by laser illumination at 10 K or raising the sample temperature to 27 K, allowing repeated measurements without the need for tip and sample preparations.

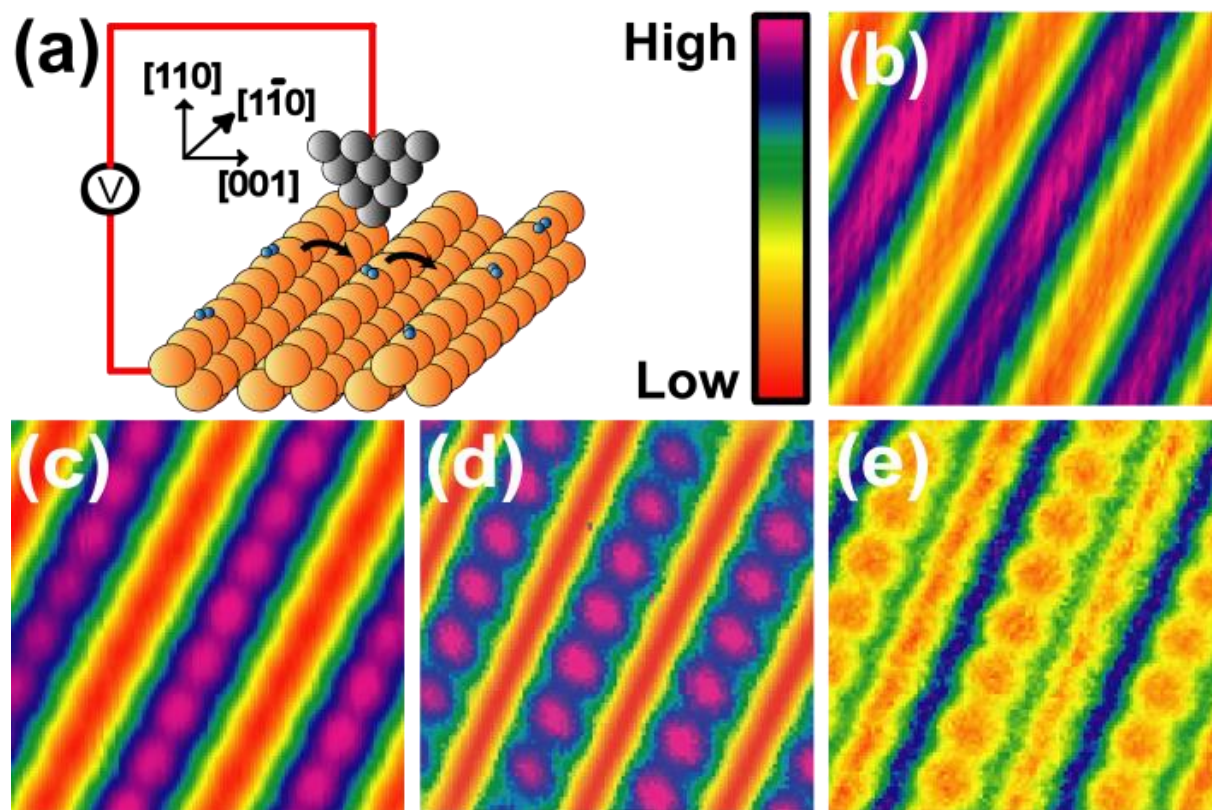
We used the Vienna Ab-initio Simulation Package (VASP) [15-17] for electronic structure calculations and structural relaxations. The spin-polarized generalized gradient approximation (GGA), using the Perdew-Burke-Ernzerhof (PBE) functional [18], was employed for the description of electronic exchange and correlation interactions. To correctly describe physisorption

systems such as $\text{H}_2/\text{Au}(110)$, the van der Waals term was considered through the vdW-DF2 functional that is implemented in VASP [19,20]. We treated H-1s and Au-5d6s as valence states and adopted the projector-augmented wave (PAW) pseudopotentials to represent their ionic cores [21,22]. The Au [110] surface was simulated with a 5-layers slab and a vacuum of about 15 Å thick. Adding a pyramid on the other side of the slab simulated the STM tip. In the lateral plane, we used a (3×3) supercell and fixed the lattice size based on the optimized lattice constant of the bulk Au ($a_{\text{Au}}=4.17$ Å). The energy cutoff of the plane-wave expansion was 700 eV, adequate for the present studies according to our test calculations. A set of $7 \times 7 \times 1$ Monkhorst-Pack [23] k-points were used for the geometry relaxation and the determination of electronic and magnetic properties at zero temperature. The tip-surface distance was adjusted by varying the length of the supercell along the z-axis. Positions of all atoms are fully relaxed according to a criterion that requires the force on each atom to be smaller than 0.01 eV/Å and the energy convergence to be better than 10^{-7} eV.

2.4 Results and Discussion

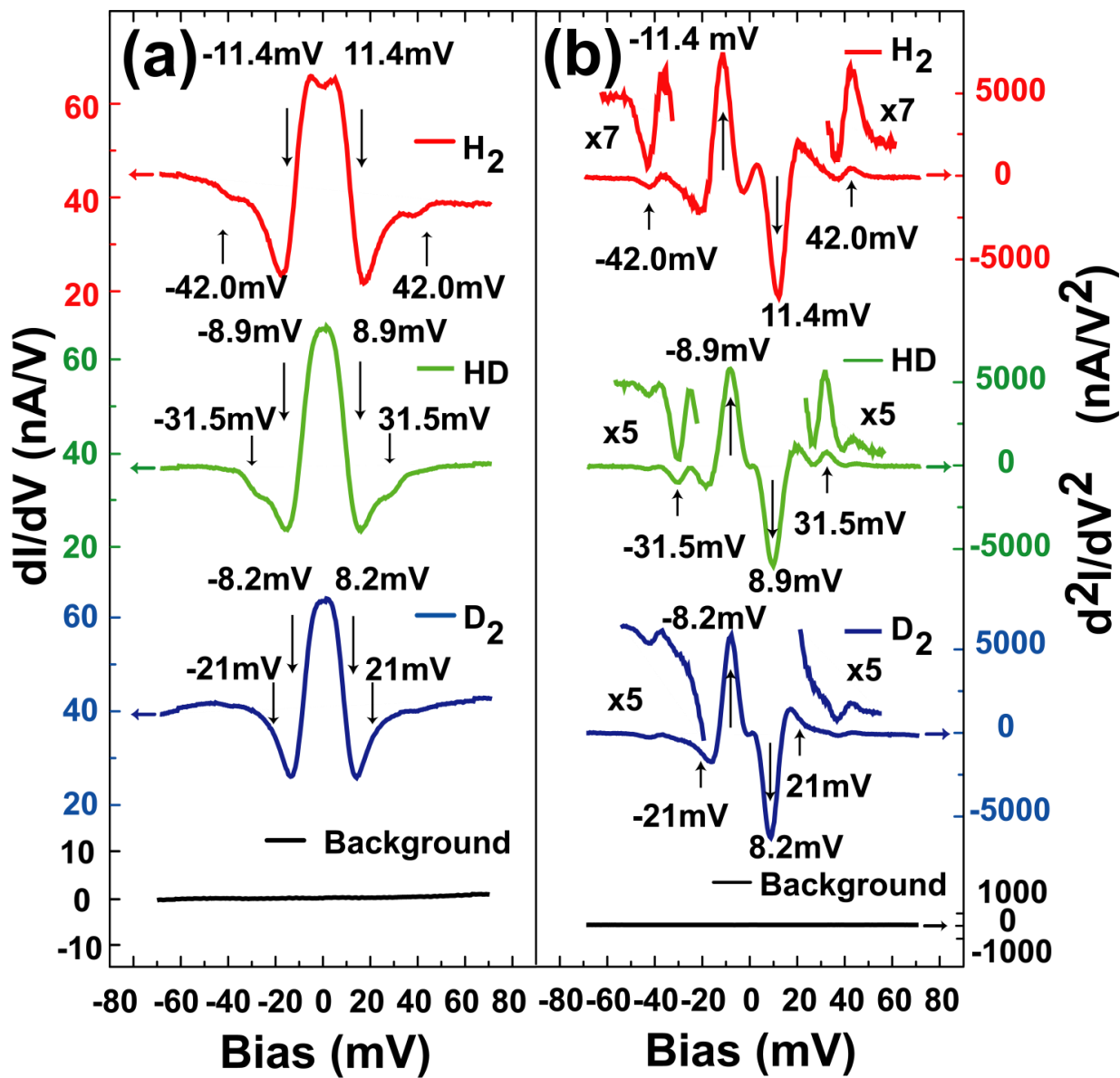
The diffusion and trapping of a molecule in the tunnel junction is illustrated in Fig. 2.1(a). The topographic STM image [Fig. 2.1(b)] taken on a hydrogen-free Au(110) surface shows a clear 2×1 reconstruction structure. After dosing H_2 , D_2 or HD, high resolution image in Fig. 2.1(c) reveals single Au atoms on atop sites; the Au atoms in the troughs remain unresolved. The dI/dV image [Fig. 2.1(d)] and d^2I/dV^2 image [Fig. 2.1(e)] also reveal atomic resolution for atop sites. The increased spatial resolution obtained after dosing H_2 , D_2 or HD indicates that a single hydrogen molecule can be trapped between the tip and an atop Au atom. In this paper, all the STS spectra were recorded above atop Au atoms.

FIG. 2.1. A hydrogen molecule trapped in the tunneling junction of STM. (a) Schematic diagram of the diffusion and trapping of a hydrogen molecule in the tunnel junction. The average lifetime of each trapped molecule in the junction is estimated to be far shorter than the response time of STM electronics. The spectroscopic signals arise from the average of many such diffusion and trapping processes. (b) STM topographic image of bare Au(110) 2×1 reconstructed surface obtained at constant current mode prior to dosing with hydrogen. Imaging conditions: tunneling gap set with sample bias $V_B=13.5$ mV and tunneling current $I_T=2$ nA. (c) STM topographic image obtain under the same conditions as (b) but after dosing with H_2 molecules. (d) dI/dV image at 0 mV bias and (e) d^2I/dV^2 image at 10 mV bias for surface adsorbed with H_2 . Tunneling gap setting conditions: $V_B = 50$ mV and $I_T = 2$ nA for (d), $V_B = 100$ mV and $I_T = 10$ nA for (e).



The rotational motion of adsorbed molecules can either be free or hindered, depending on the depth of the adsorption well. Previous STM studies have investigated the rotational motion of molecules stably adsorbed on the surface and can be imaged [24-26]. In these studies, the molecules are highly constrained to be within the adsorption well and the rotations are described as hindered vibrational modes. However, if the adsorption potential well is shallow, the rotational motion of the adsorbed molecule is “unhindered” [27] and is characteristic of a rigid three-dimensional (3D) free rotor. The rotational energy is given by $j(j+1)\hbar^2/2\mu r_b^2$, where $j=0,1,2,\dots$, μ is the reduced mass of the molecule, and r_b is the distance between the two atoms in the molecule (the bond length for H_2). In the STS spectra taken on H_2 , a step change in dI/dV spectrum is observed [Fig. 2.2(a)], with a corresponding peak in the d^2I/dV^2 spectrum [Fig. 2.2(b)] at 42.0 mV. This energy agrees with the $j=0\rightarrow 2$ rotational excitation of a para- H_2 as a 3D rigid rotor, indicating that the H_2 molecules on Au(110) behave like in the gaseous phase. For the HD, this inelastic rotational signal shifts down to 31.5 mV, which is 0.75 times the measured transition energy of H_2 , in agreement with the value of 3/4 according to the 3D rigid rotor model. Since the two atoms in HD are distinguishable, the $j=0\rightarrow 1$ excitation is allowed. However, this excitation is difficult to resolve since its energy is expected to be at 10.5 mV, where the signal is dominated by the $\nu=0\rightarrow 1$ vibrational transition. For the same reason, the $j=0\rightarrow 2$ excitation energy of ortho- D_2 at 21 mV is similarly difficult to be resolved. On the other hand, the $j=1\rightarrow 3$ rotational excitation at 70 mV for ortho- H_2 and 35 mV for para- D_2 is not visible in the STS spectra. These results are in agreement with prior measurements by electron energy loss spectroscopy (EELS), showing that hydrogen molecules are weakly adsorbed on noble metal surfaces at low temperature and rapidly convert into the $j=0$ state (the para- H_2 or ortho- D_2) [9,25,29]. Thus the presence of ortho- H_2 or

FIG. 2.2. Tunneling spectra taken before and after dosing molecular hydrogen or its isotopes. The tunneling gap is set with $V_B=50$ mV and $I_T=2$ nA for all the spectra. The bias for the x-axis in the spectra has been shifted up by 1 mV to compensate for instrumental offset. (a) From the top to the bottom: dI/dV spectra of H_2 , HD, D_2 , and clean gold surface (Background). (b) From the top to the bottom: d^2I/dV^2 spectra of H_2 , HD, D_2 , and clean gold surface (Background). The magnified line shapes for the rotational excitation are also presented. The excitation energies are marked by arrows. The signal at ± 42.0 mV in H_2 spectra and the signal at ± 31.5 mV in HD spectra are assigned to the $j=0 \rightarrow 2$ rotational excitation. The small structure around ± 42 mV in HD and D_2 spectra is attributed to contamination from coadsorption of background H_2 in the vacuum chamber. The strong signals at ± 11.4 mV, ± 8.9 mV, ± 8.2 mV in the spectra for H_2 , HD, D_2 are assigned to the $\nu=0 \rightarrow 1$ vibrational excitation within the physisorption potential well.

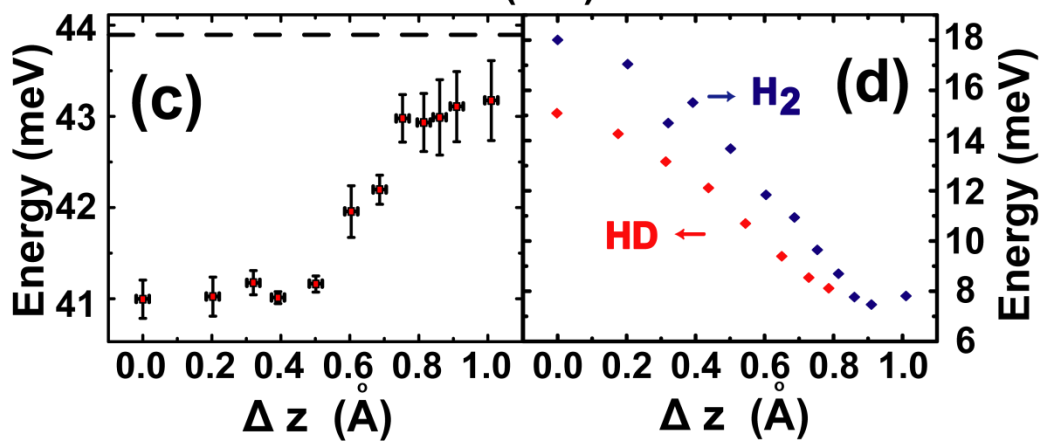
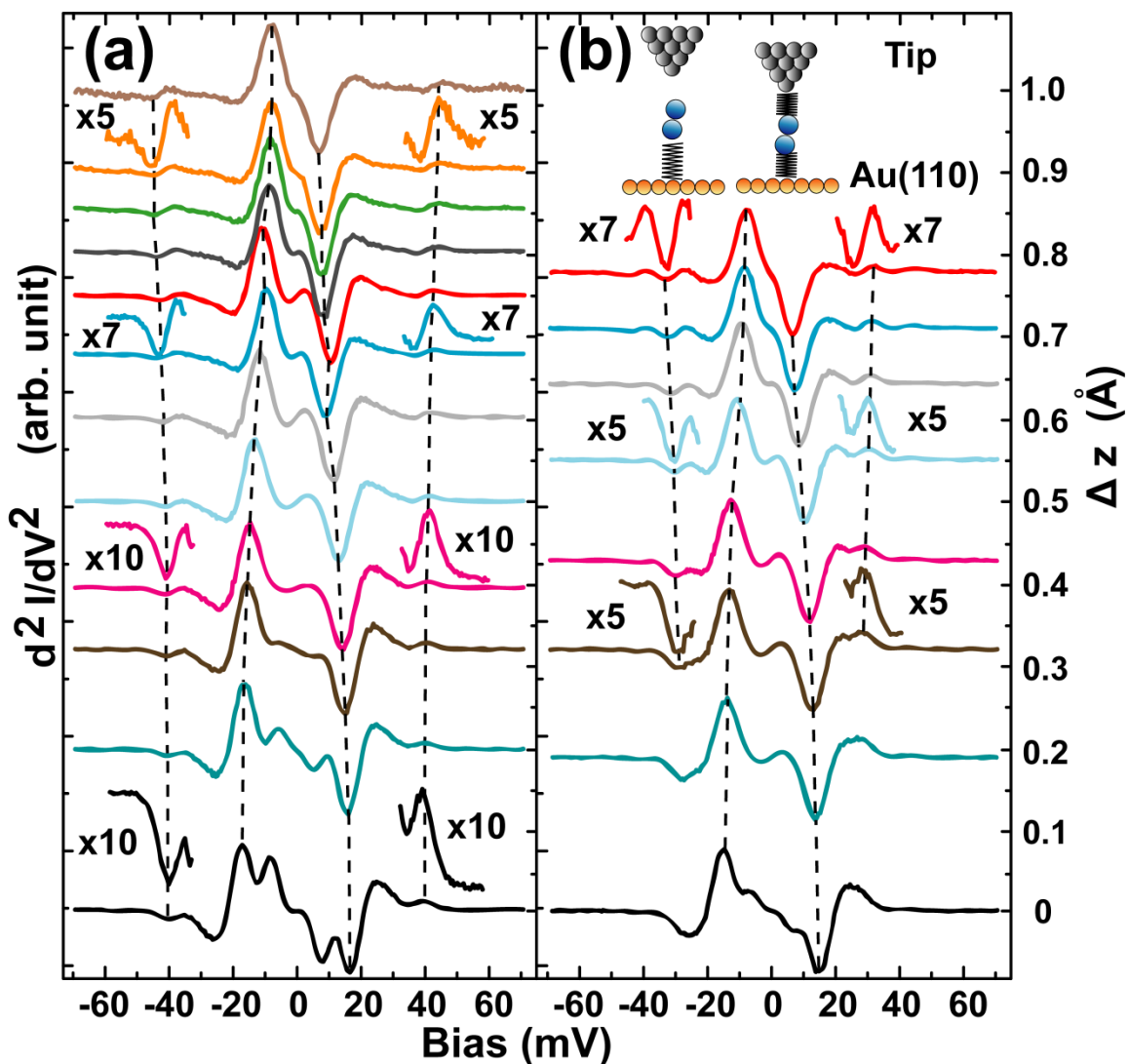


para-D₂ is unlikely on Au(110) at 10 K. Nevertheless, our data for H₂ and HD are sufficient to indicate that molecular hydrogen on Au(110) behaves as a 3D rigid rotor.

The strong signals at lower energies in the tunneling spectra are assigned to the vibrational excitations in the physisorption potential well. In the harmonic approximation, the vibration energies are given by $\hbar\nu(v+1/2)$ with $v=0,1,2,\dots$. In the tunneling spectra of H₂, the large step down at 11.4 mV in the dI/dV spectrum [Fig. 2.2(a)] and the corresponding asymmetric dip in the d²I/dV² spectrum [Fig. 2.2(b)] are assigned to the $v=0\rightarrow 1$ excitation of the hydrogen vibrational motion bouncing between the tip and substrate. In the tunneling spectra of HD and D₂, the $v=0\rightarrow 1$ transition energy is shifted down to 8.9 mV and 8.2 mV, respectively. The ratios of these transition energies are 1.3 between H₂ and HD and 1.4 between H₂ and D₂, in agreement with the quantum harmonic oscillator.

The rotational energy is directly related to the principal moment of inertia of the molecule and, therefore, to its structure [30]. Rotational spectroscopy with the STM can be used to probe changes in the structure of a single molecule due to its coupling to its environment. The rotational excitation energies in Fig. 2.2 are slightly smaller than the theoretical result for a free molecule (42.0 vs. 43.9 mV for H₂ and 31.5 vs. 33.1 mV for HD) or the experimental data measured for an ensemble of molecules by EELS (44 mV for H₂ [9,31]). These deviations are presumably caused by changes in the molecular structure due to coupling of the molecule to the tip. The effect of this coupling can be systematically investigated by varying the tip-substrate separation which is controlled by setting the sample bias and tunneling current. As the sample bias decreases from 120 mV to 5 mV while keeping the tunneling current constant at 2 nA, the tip is moved toward the surface by approximately 1 Å (the tip-substrate separation changes from 7.5 Å to 6.5 Å). Both the vibrational and rotational excitation energies change during this process. The $v=0\rightarrow 1$ vibrational

FIG. 2.3. IETS at different tip-substrate separations. (a-b) d^2I/dV^2 spectra taken at different tip-substrate separation for H_2 (a) and HD (b). The sample bias V_B is changed from 5 mV (bottom) to 120 mV (top) in (a) and from 5 mV (bottom) to 70 mV in (b). I_T is kept at 2 nA for all these spectra. A z-V curve is measured to convert the change in V_B to the corresponding change in the tip-substrate separation (Δz). The tunneling gap distance at $V_B=5$ mV and $I_T=2$ nA is used as the reference point ($\Delta z=0$). The uncertainty in Δz is around 0.095 Å. The shiftings of the rotational and vibrational excitation energies are indicated by the dashed lines. The magnified line shapes of the rotational excitation are also presented. (c) The $j=0 \rightarrow 2$ excitation energy increases from 41 mV to 43 mV as Δz increases by 1 Å. The horizontal dashed line indicates for reference the excitation energy of a free molecule. (d) The $\nu=0 \rightarrow 1$ excitation energy decreases from 18 mV to 7.5 mV as Δz increases by 1 Å for H_2 , and from 15 mV to 8mV as Δz increases by 0.8 Å for HD.

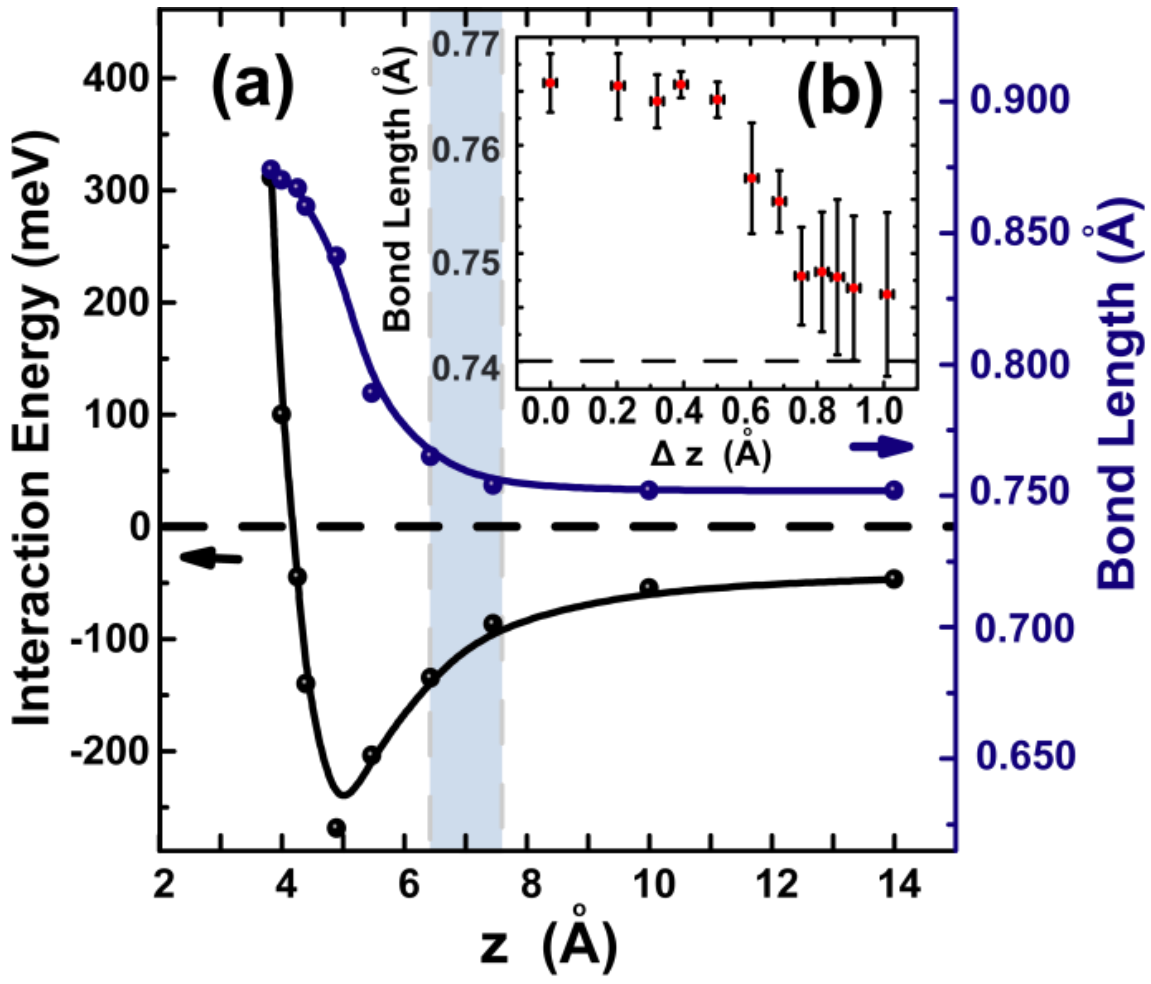


excitation energy of H₂ increases from 7.5 mV to 18 mV [Fig. 2.3(d)]. The tunneling spectra for HD show similar trend when the tip-substrate separation is changed [Fig. 2.3(b)]. The increase of vibration energy suggests an increased bonding of the molecule to the substrate, which weakens the H-H bond strength and increases the bond length as predicted by theoretical calculations [32, 33]. DFT calculations of the adsorption energy and H-H bond length at different tip-substrate separations have been performed [Fig. 2.4(a)] using the Viena ab-initio simulation package (VASP) at the level of vdW-DF2. A Morse potential like adsorption energy curve is revealed which further confirms that van der Waals interactions are dominant in this weakly bonding system. According to the calculation, the H-H bond length increases from 0.750 Å to 0.765 Å when the tip-substrate separation decreases from 7.5 Å to 6.5 Å. In agreement with the DFT calculations, the rotational excitation energy of H₂ decreases from 43 mV to 41 mV [Fig. 2.3(c)] as the tip-substrate separation decreases by ~1 Å, indicating that the H-H bond length increases from 0.746 Å to 0.766 Å [Fig. 2.4(b)]. DFT calculations also identified the observed vibrational mode as the bouncing motion of H₂ confined between the Au(110) surface and the tip.

2.5 Conclusions

In summary, the STM has been extended to the study of the rotational excitations of weakly adsorbed molecules, in addition to the detection of vibrational transitions. Rotational spectroscopy at the single molecule level opens a new avenue for chemical identification and measurement of the bond length in a single bond. By squeezing a trapped hydrogen molecule in the tip-substrate junction by decreasing the dimension of the nanocavity, structural changes in a single molecule can be observed by altering the potential experienced by the molecule.

FIG. 2.4. DFT calculations. (a) DFT calculations of the interaction energy between the trapped molecule and the tunneling junction, and H-H bond length at different tip-substrate separation. The blue shaded area indicates the approximate range probed by STM. (b) The H-H bond length, derived from the measured $j=0 \rightarrow 2$ excitation energies, decreases from 0.766 Å to 0.746 Å as Δz increases by 1 Å. The dashed line indicates for reference the H-H bond-length of a free molecule.



2.6 Bibliography

- [1] R. C. Jaklevic and J. Lambe, Phys. Rev. Lett. **17**, 1139 (1966).
- [2] E. B. Wilson Jr., Science **162**, 59 (1968).
- [3] P. O. Stoutland, R. B. Dyer, and W. H. Woodruff, Science **257**, 1913 (1992).
- [4] R. S. McDonald, Anal. Chem. **58**, 1906 (1986).
- [5] P. R. Griffiths, Science **222**, 297 (1983).
- [6] K. K. Kohli, Gordon Davies, N. Q. Vinh, D. West, S. K. Estreicher, T. Gregorkiewicz, I. Izeddin, and K. M. Itoh, Phys. Rev. Lett. **96**, 225503 (2006).
- [7] C. Schröter, K. Kosma, and T. Schultz, Science **333**, 1011 (2011).
- [8] B. C. Stipe, M.A. Rezaei, and W. Ho, Science **280**, 1732 (1998).
- [9] K. Svensson and S. Andersson, Surf. Sci. **92**, L40 (1997).
- [10] J. A. Gupta, C. P. Lutz, A. J. Heinrich, and D. M. Eigler, Phys. Rev. B **71**, 115416 (2005).
- [11] J. R. Hahn and W. Ho, Phys. Rev. Lett. **87**, 196102 (2001).
- [12] C. Weiss, C. Wagner, C. Kleimann, M. Rohlfing, F. S. Tautz, and R. Temirov, Phys. Rev. Lett. **105**, 086103 (2010).
- [13] W. H. A. Thijssen, D. Djukic, A. F. Otte, R. H. Bremmer, and J. M. van Ruitenbeek, Phys. Rev. Lett. **97**, 226806 (2006)
- [14] B. C. Stipe, M. A. Rezaei, and W. Ho, Rev. Sci. Instrum. **70**, 137, (1999).
- [15] G. Kresse and J. Hafner, Phys. Rev. B **47**, 558 (1993).
- [16] G. Kresse and J. Hafner, Phys. Rev. B **49**, 14251 (1994).
- [17] G. Kresse and J. Furthmuller, Phys. Rev. B **54**, 11169 (1996).
- [18] J. P. Perdew, K. Burke, and M. Ernzerhof, Phys. Rev. Lett. **77**, 3865 (1996).
- [19] J. Klimeš, D. R. Bowler, and A. Michaelides, Phys. Rev. B **83**, 195131 (2011).

- [20] J. Klimeš, D. R. Bowler, and A. Michaelides, *J. Phys.: Cond. Matt.* **22**, 022201 (2010).
- [21] P. E. Blochl, *Phys. Rev. B* **50**, 17953 (1994).
- [22] G. Kresse and D. Joubert, *Phys. Rev. B* **59**, 1758 (1999).
- [23] H. J. Monkhorst and J. D. Pack, *Phys. Rev. B* **13**, 5188 (1976).
- [24] B. C. Stipe, M.A. Rezaei, and W. Ho, *Science* **279**, 1907 (1998).
- [25] L. J. Lauhon and W. Ho, *J. Chem. Phys.* **111**, 5633 (1999).
- [26] J. K. Gimzewski, C. Joachim, R. R. Schlittler, V. Langlais, and H. Tang, I. Johansen, *Science* **281**, 531 (1998).
- [27] I. F. Silvera, *Rev. Mod. Phys.* **52**, 393 (1980)
- [28] E. Ilisca, *Prog. Surf. Sci.* **41**, 217 (1992).
- [29] P. Avouris, D. Schmeisser, and J. E. Demuth, *Phys. Rev.Lett.* **48**, 199 (1982).
- [30] B. C. Dian, G. G. Brown, K. O. Douglass, F. S. Rees, J. E. Johns, P. Nair, R. D. Suenram, and B. H. Pate, *Proc. Natl. Acad. Sci. U.S.A.* **105**, 12696 (2008).
- [31] K. Svensson and S. Andersson, *Phys. Rev. Lett.* **78**, 2016 (1997). .
- [32] S. Sakong and A. Groß, *Surf. Sci.* **525**, 107 (2003).
- [33] A. Groß, *Appl. Phys. A* **67**, 627 (1998).

Chapter 3

Rotational Spectromicroscopy: Imaging the Orbital Interaction between Molecular Hydrogen and an Adsorbed Molecule

3.1 Abstract

A hydrogen molecule can diffuse freely on the surface and be trapped above an adsorbed molecule within the junction of a scanning tunneling microscope. The trapped dihydrogen exhibits the properties of a free rotor. Here we show that the intermolecular interaction between dihydrogen and Mg-porphyrin (MgP) can be visualized by imaging $j=0$ to 2 rotational excitation of dihydrogen. The interaction leads to a weakened H-H bond and modest electron donation from the dihydrogen to the lowest unoccupied molecular orbital of MgP, a process similarly observed for the interaction between dihydrogen and an adsorbed Au atom.

3.2 Introduction

The nature of the interaction between molecules underlies the understanding of chemistry in diverse fields of chemical synthesis, drug design and molecular electronics [1-3]. The strong covalent bond between molecules has been manipulated and characterized at the single molecule level using the scanning tunneling microscope (STM) [4,5]. The real-space microscopic features possibly resembling the weak intermolecular hydrogen bonds have also been observed using non-contact atomic force microscopy [6], scanning tunneling hydrogen microscopy (STHM) [7], and inelastic tunneling probe (itProbe) [8]. However, the application of real-space visualization of chemical bonding could be enhanced by extending the control and quantifying the intermolecular interactions [9], especially for non-planar geometries between the interacting molecules.

Orbital hybridization and charge transfer are two key mechanisms underlying the interaction between two molecules [4]. The magnesium porphyrin (MgP) molecule can participate as an electron acceptor. In one such instance, a negative ion (MgP^-) is formed by tunneling electrons from the STM tip. This single molecule electron transfer is reversible and can be controlled by choosing the bias between STM tip and substrate [10,11]. In contrast, molecular hydrogen can be an electron donor. Dihydrogen cations (H_2^+) are formed abundantly in the universe from ionization of neutral hydrogen molecules by cosmic rays. The electron from the occupied σ orbital of neutral H_2 ($\sigma_{\text{H-H}}$) can be transferred to an acceptor if the two molecules have a favorable geometry [12, 13]. Consequently, MgP and H_2 can potentially form a donor-acceptor pair and investigation of the interaction between them may reveal insights into the mechanism of intermolecular hybridization and charge transfer.

STM has been used effectively to investigate and manipulate single atoms and molecules. The STM tip and substrate form a nano-cavity in which molecular hydrogen can be trapped at low temperature by van der Waals forces [14-17]. The trapped H_2 is sensitive to its local environment and the spatial variation in the potential energy surface can be quantified by changes in its rotational and vibrational energies [14]. Consequently, we can use the trapped H_2 as a sensor of its environment, such as over another adsorbed molecule to investigate the intermolecular interaction by monitoring the rotational excitation of H_2 . The trapping potential moves with the scanning tip. Spatial imaging of the intermolecular interaction between the trapped hydrogen and the underlying molecule can be obtained by rotational spectromicroscopy.

In this letter, we probe the $j=0 \rightarrow 2$ rotational excitation of a trapped H_2 over neutral MgP and anionic MgP^- molecules adsorbed on bi-layer alumina (Al_2O_3) grown on NiAl(110) surface. The Al_2O_3 serves as a decoupling layer to suppress the orbital hybridization between adsorbed

molecules and the metal substrate [Fig. 3.1(a)]. The rotational and vibrational spectra of H₂ trapped above a Au adatom on NiAl(110) are also investigated for comparison to MgP adsorbed on alumina. The rotational and vibrational excitation energies are measured by inelastic electron tunneling spectroscopy (IETS) with the STM. The existence of the rotational spectra and the measured energies suggest that the trapped H₂ behaves like a free three-dimensional (3D) rigid rotor, freely translating and rotating on the surface at 10 K. However, the rotational and vibrational energies and line shapes in the d^2I/dV^2 spectra vary as the trapped H₂ experiences spatially dependent interactions with the underlying surface.

3.3 Methods

The experiments were performed using a home-built STM operating at 10 K and a base pressure of 3×10^{-11} Torr [18]. The preparation of the NiAl(110) surface and Al₂O₃ patches follows previously reported procedures [19]. The Ag tip was electrochemically etched. The clean surface at 10 K was dosed *in situ* with MgP and Au. As hydrogen molecules have limited residence time on the Al₂O₃/NiAl(110) surface at 10 K, a background pressure of H₂ is kept at 1×10^{-10} Torr throughout the experiment to maintain a constant population of adsorbed H₂ on the surface following an initial dose at 5×10^{-10} Torr for 5 min. A bias voltage V_B is applied to the sample with the tip connected to the current amplifier at virtual ground.

The calculations are performed using the plane-wave based Vienna ab initio simulation package (VASP) [20-22]. The interaction between the ion and core electrons is described by the projector augmented wave (PAW) method [23]. Plane waves with an energy cutoff of 500 eV are used to expand the Kohn-Sham wave functions. The Ag STM-tip is constructed with 29 Ag atoms, consisting of two Ag(111) layers and an Ag adatom [Fig. 3.4(a)]. To simulate the adsorption of H₂

molecule in the junction of Ag STM-tip and MgP molecule, we use a cubic supercell of 20 Å in each dimension. To correctly describe the adsorption of H₂ in the junction, the van der Waals correction is included using the optB86b-vdW functional [24,25]. For the large supercell, single Gamma point is used to sample the small Brillouin zone during geometrical optimization, whereas a set of 3×3×3 Monkhorst-Pack k-points is employed [26] for the electronic structure calculations. In our DFT calculations, the distance between the tip and MgP varies from 6.0 to 4.5 Å along the tunneling gap. Most results we discuss in the text are for the tip-molecule distance of 4.5 Å, which best reproduces the experimental conditions.

3.4 Results and Discussion

Due to the inhomogeneity of the alumina film grown on NiAl(110), the MgP molecules adsorb in a variety of geometries, including those which can become negatively charged by capturing a tunneling electron from the STM tip [11]. The differential conductance (dI/dV) spectra measured over a chargeable MgP show hysteresis during forward and backward scans (ramping V_B up and down). The step-down in the conductance [red vertical arrow in Fig. 3.1(b)] appears after the onset of the lowest unoccupied molecular orbital (LUMO, 0.5 V for the molecule shown in Fig. 3.1), indicating that an electron transfer to MgP has occurred through the injection of an electron into the LUMO. The MgP⁻ is reverted back to the neutral molecule by transferring an electron from its singly occupied molecular orbital (SOMO) to the tip at a negative bias, as indicated by the step-down in the conductance when the bias is ramped backward [black vertical arrow in Fig. 3.1(b)]. Because the STM images closely follow the electronic structure, the topographic images taken at 0.5 V [LUMO, Fig. 3.2 (a)] for MgP and 0.9 V [singly unoccupied molecular orbital (SUMO),

FIG. 3.1. Reversible electron transfer to a single MgP molecule interacting with H₂ in a double barrier tunnel junction of the STM. (a) Schematic diagram of a single molecule double-barrier junction with temporarily trapped H₂. The spectroscopic signal arises from the average of many diffusion and trapping processes for H₂. (b) dI/dV spectra measured over a MgP molecule undergoing reversible single electron transfer in the geometry sketched in (a). The inset shows the topographic image of the charged molecule taken with a gap set with $V_B = 1.5$ V and $I_T = 0.1$ nA. The position for recording the dI/dV spectra is marked in the topographic image. The red curve is the dI/dV spectrum taken when the sample bias is ramped from low to high (Forward) while the black curve is taken with the bias ramped from high to low (Backward). The two vertical arrows mark the positions of sudden conductance change during the forward and backward scans, corresponding to the charging and discharging of the molecule, respectively. The onset of the LUMO of MgP is around 0.5 V, and the onsets for the SUMO and SOMO of MgP⁻ are around 0.6 V and -0.5 V, respectively.

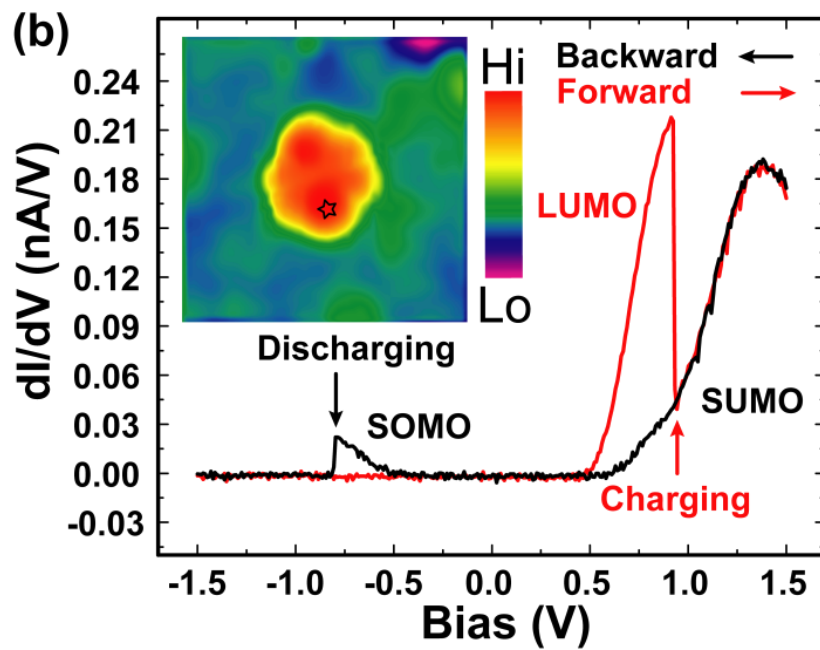
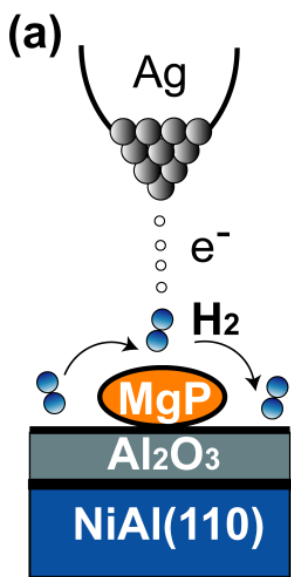
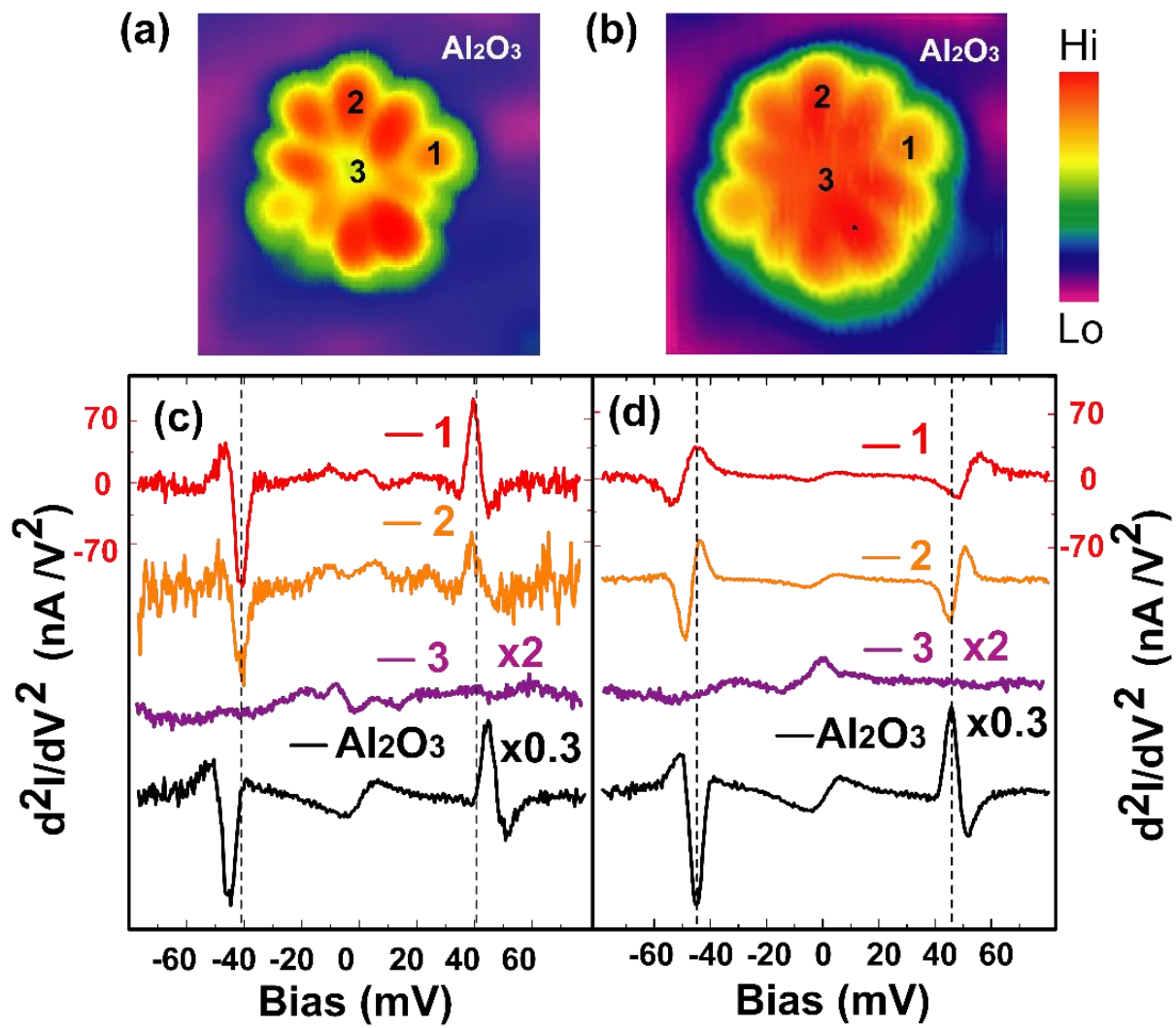


Fig. 3.2(b)] for MgP⁻ show similar 10-lobes patterns that are in agreement with density function theory (DFT) calculations [27].

After dosing H₂, IETS measurement over the bare alumina surface shows an inelastic excitation signal at 45.1 meV. This signal is attributed to the j=0→2 rotational excitation of molecular hydrogen and has previously been confirmed by isotopic substitution [14, 28]. When the tip is located over one of the prominent lobes in the LUMO of MgP, the j=0→2 rotational excitation energy shifts to 42.0 meV. The change in rotational excitation energy can be an indicator of a change in the H-H bond length [14]. The downshift of the rotational excitation indicates a stretched and weakened H-H bond, in response to variations in the interaction potential surface. If the tip is moved toward the center of MgP, spectral features in the IETS become progressively weaker and are not resolved directly over the center of MgP. DFT calculations suggest the 3D rotor behavior of H₂ can only exist over the rim of MgP molecule. The rotational motion is suppressed at the center of MgP due to the large anisotropy energy between the vertical and horizontal adsorption geometries of H₂ in the tunnel junction, causing the absence of the rotational signal in IETS. Variation in the measured rotational excitation energy is not significant over different outer lobes of a MgP molecule [Fig. 3.2(c)]. However, variation in the intensity between the lobes indicates that the interaction between hydrogen and MgP is affected by the anisotropy in the adsorption geometry of MgP.

Rotational imaging reveals the role of molecular orbitals in the interaction between H₂ and MgP by measuring the spatial distribution of the second derivative signal d^2I/dV^2 at the rotational energy of 42 meV (Fig. 3). The junction gap is set with 50 mV sample bias and 0.1 nA tunneling current, followed by disabling the feedback and decreasing the bias to 42 mV to record the second derivative rotational signal which is proportional to the second harmonic output of the lock-in

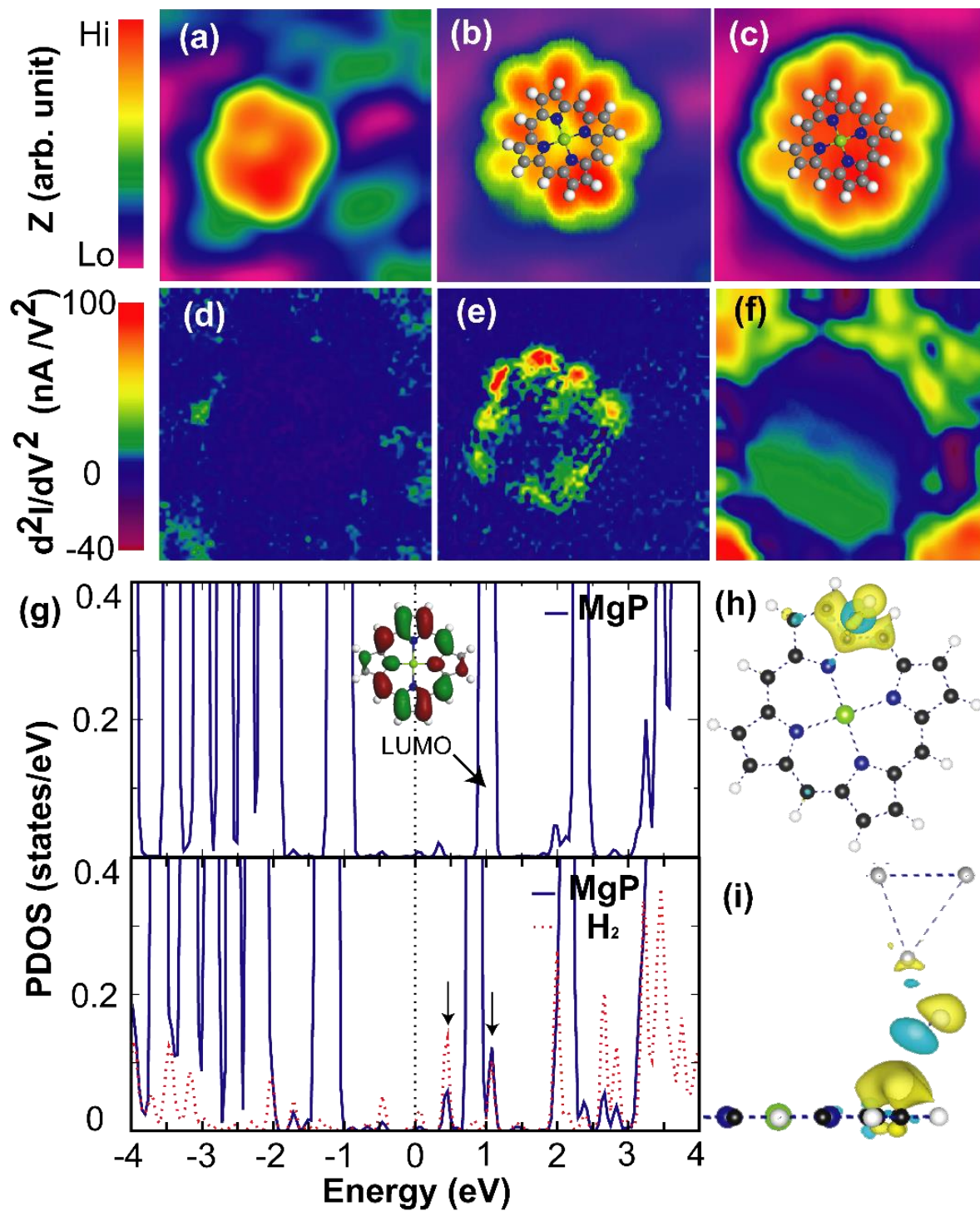
FIG. 3.2. Rotational spectra of single H_2 molecule interacting locally with MgP measured by STM-IETS. (a-b) Topographic images taken at the onset of MgP LUMO (a) and the onset of MgP^- SUMO (b). The set points are $V_B = 500$ mV, $I_T = 0.1$ nA for (a) and $V_B = 800$ mV, $I_T = 0.1$ nA for (b). (c) The IETS spectra of trapped H_2 taken over different positions over MgP and alumina, as marked in (a). The vertical dashed line indicates the energy of $j=0 \rightarrow 2$ rotational excitation of H_2 measured over position 1 of MgP. For all the spectra, the tunneling gap is set with $V_B = 50$ mV and $I_T = 0.1$ nA, and the sample bias is modulated at 345 Hz and 5 mV rms. The spectra are the result of an average of 10 scans. (d) The IETS spectra taken under same set point conditions as in (c) for positions over MgP^- as marked in (b). The spectra are the result of an average of 50 scans. The vertical dashed line indicate the $j=0 \rightarrow 2$ rotational excitation of H_2 measured over alumina background.



amplifier. The rotational image at 42 mV [Fig. 3.3(e)] shows a multi-lobes pattern that closely resembles the LUMO image [Fig. 3.3(b)], but is significantly different from the constant-current topographic image taken at 50 mV and 0.1 nA (same set point as the rotational image) [Fig. 3.3(a)]. The spatial contrast can only be observed with the sample bias in resonance with the rotational excitation. The off resonance image at 37 mV is nearly featureless [Fig. 3.3(d)]. The spatial similarity between the hydrogen rotational image at 42 mV and the MgP LUMO image at 500 mV indicates that the intermolecular hybridization of MgP and H₂ is dominated by the interaction between MgP LUMO and hydrogen orbitals.

The role of charge transfer between MgP and H₂ is further investigated by rotational analysis of the charged MgP⁻. The $j=0 \rightarrow 2$ rotational excitation signal in the IETS over MgP⁻ is significantly different than over MgP and alumina. The intensity of the rotational excitation signal is lower, possibly because the interaction between MgP⁻ and H₂ is less attractive. The line shape of the rotational feature in the d^2I/dV^2 spectrum at positive bias changes from a peak with a side dip [Fig. 3.2(c)] into a dip with a side peak [Fig. 3.2(d)] with the expected behavior at negative bias, which is possibly due to the change in the coupling of the inelastic and elastic tunneling processes or the local variation of surface potential [29, 30]. Aside from the changes in signal intensity and line shape, the excitation energy doesn't change significantly when the tip is moved from alumina to over MgP⁻. The rotational image at 45 mV [Fig. 3.3(f)] does not reveal clear features within the molecule. The mismatch between the rotational and the SUMO images demonstrates that the singly unoccupied orbital contributes negligibly to the interaction between H₂ and MgP⁻.

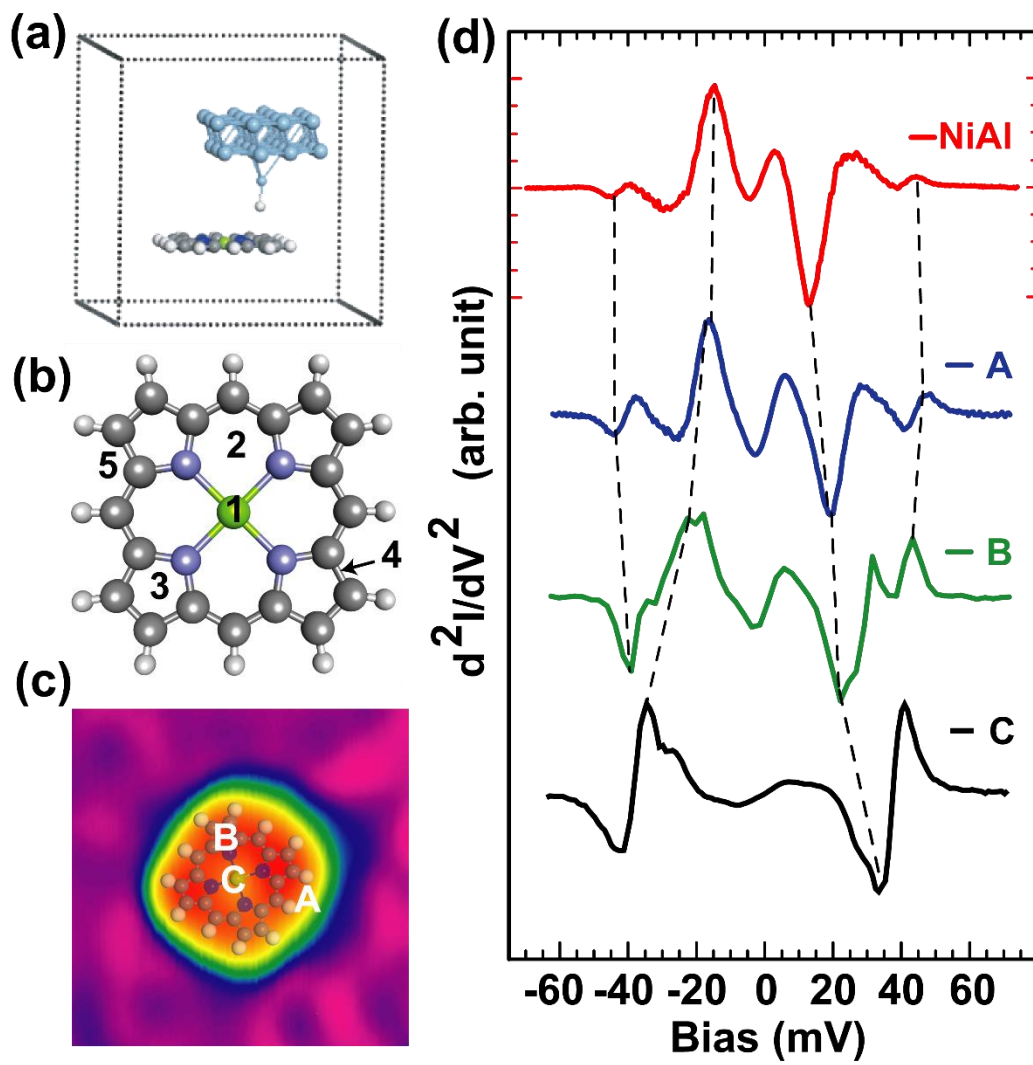
FIG. 3.3 Single molecule rotational imaging. (a) Constant current topographic image of MgP taken at $V_B = 50$ mV, $I_T = 0.1$ nA. (b-c) Topographic images showing the (b) LUMO of MgP imaged at $V_B = 500$ mV, $I_T = 0.1$ nA, and (c) SUMO of MgP^- imaged at $V_B = 800$ mV, $I_T = 0.1$ nA. The structure of the molecule is superposed on the images. (d) d^2I/dV^2 images taken at 37 mV which is off-resonance of the $j=0 \rightarrow 2$ rotational excitation energy of H_2 . The image doesn't show obvious structure. (e) d^2I/dV^2 image taken at 42 mV on MgP showing the multi-lobes feature, and additionally the overall size of the image closely follows the molecular skeletal structure superimposed in (b) and (c). (f) d^2I/dV^2 on-resonance image taken at 45 mV on MgP^- . The image also does not reveal clear structure. (g) Calculated partial density of states (PDOS) of tip-MgP junction (top) and tip- H_2 -MgP junction with configuration (5-d) in TABLE 3.1. The calculated image of the LUMO for MgP is shown in the inset. The two new features of MgP states (blue solid peaks) in resonance with H_2 states (red dashed peaks) are indicated by arrows in the bottom panel. (h) top view and (i) side view of the charge density difference in tip- H_2 -MgP junction. Yellow region indicates charge accumulation while blue regions indicate charge depletion. The value of isosurface for the charge difference is 0.0004 bohr^{-3} . The results repeat in the other three quadrants of the molecule.



The major difference in the interaction with H₂ is that MgP is an electron acceptor while MgP⁻ is an electron donor. In contrast to the SUMO of MgP⁻, the LUMO of MgP readily accepts an electron. In the interaction of H₂ with MgP, electrons in the σ_{H-H} partially transfer to the LUMO of MgP [31]. DFT calculations of the projected density of state (PDOS) [Fig. 3.3(g)] and charge density difference [Fig. 3.3(h) and 3(i)] have been performed for the tip-H₂-MgP junction. The Fermi level shifts towards the LUMO when interacting with H₂, compared to the H₂-free junction. Two extra peaks [two vertical arrows in Fig 3(g)] next to the LUMO of MgP confirm the hybridization between the MgP-LUMO and H₂ orbitals. Calculated charge density difference confirms the electron transfer from H₂ to MgP. The spatial distribution of the transferred charge closely follows the LUMO lobes [Fig. 3.3(h) and 3(i)].

The intensity in the rotational image [Fig 3(e)] is observed to lie in the outer region of the molecule. The $j=0 \rightarrow 2$ rotational excitation signal in the IETS becomes progressively weaker and is not detected over the center of MgP. The Ag tip is situated at five positions over the MgP molecule, as indicated in Fig. 3.4(b), to investigate the interaction between the H₂ and MgP with DFT. The results calculated for the interaction are tabulated in TABLE. S1. The adsorption energy of H₂ (E_{ad}) is determined by $E_{ad} = E_{H_2/tip+MgP} - E_{tip+MgP} - E_{H_2}$, where $E_{H_2/tip+MgP}$, $E_{tip+MgP}$, and E_{H_2} are the total energies of tip-H₂-MgP junction, tip-MgP junction and isolated H₂, respectively. The positions of atoms in the Ag tip and the MgP molecule are fixed during the optimization of the adsorption configuration of H₂. Calculations indicate that the adsorption energy of H₂ sensitively depends on the orientation of H-H bond at positions 1-4, where the rotation of H₂ is effectively hindered due to large energy anisotropy. At the edge of MgP (position 5), H₂ interacts with MgP but may still freely rotate due to the smallest energy anisotropy. Therefore, the intensity of the rotational image of MgP [Fig 3(e)] is very low near the center of MgP.

FIG. 3.4. MgP over NiAl surface. (a) Schematic diagram of the structural model of DFT calculations. The light blue, gray, dark blue, green, and white balls represent Silver, Carbon, Nitrogen, Magnesium and Hydrogen atoms, respectively. (b) The five positions where the adsorption energy of H₂ over MgP are calculated. (c) The constant current topographic image of a MgP molecule adsorbed on NiAl(110) surface. $V_B = 50$ mV, $I_T = 0.1$ nA (d) The d^2I/dV^2 spectra taken with a trapped H₂ at different positions over a MgP molecule adsorbed on NiAl(110) as indicated by positions A, B, and C in (c), and over the NiAl substrate. The set point is $V_B = 50$ mV, $I_T = 1$ nA.

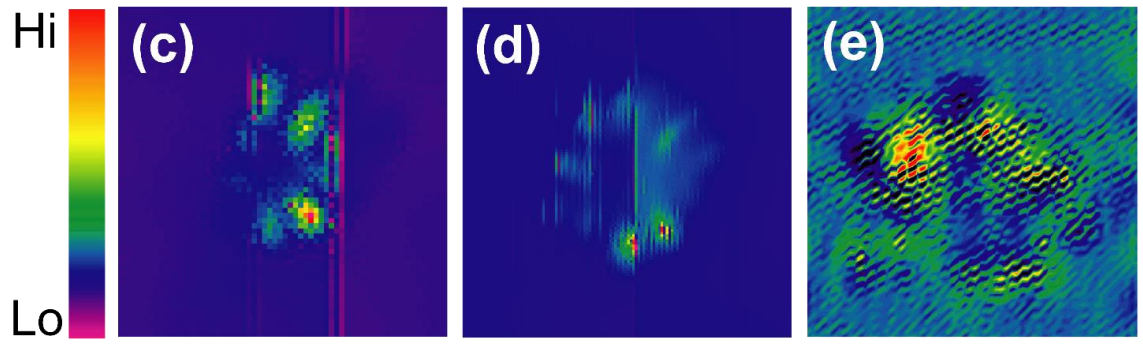
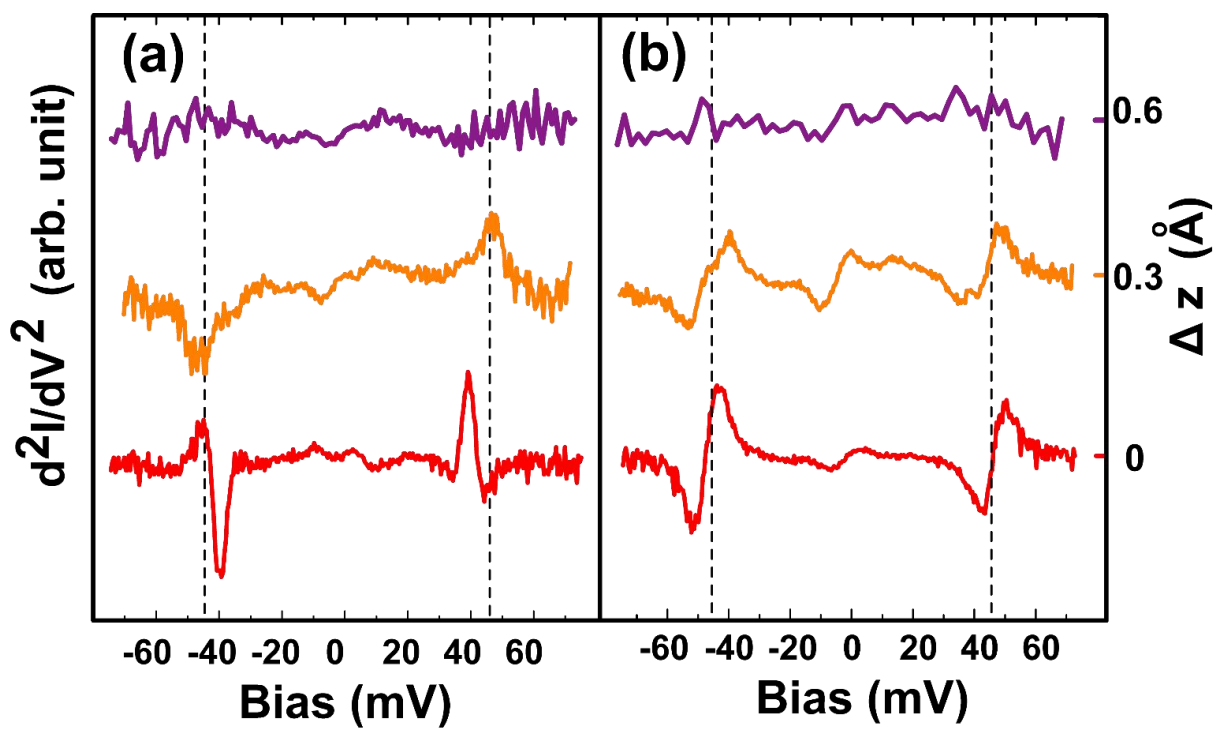


The d^2I/dV^2 spectra of H_2 over MgP adsorbed on NiAl(110) are presented in Fig. 3.4(d). Beside the rotational signal around 44 mV, the spectra also show strong vibrational features of H_2 over MgP. The vibrational energy significantly increases as the tip moving from the edge toward the center of MgP; this trend is also observed as the tip moving toward the center of an Au atom adsorbed on the NiAl(110) surface. The weak H_2 rotational feature is eventually overwhelmed by the vibrational signal over the Mg atom. The increase of vibration energy can be correlated with an increase of H_2 adsorption energy, which would hinder the rotational motion of H_2 near the center of MgP, leading to the suppression of the rotational excitation signal. Since the selection rule of STM-IETS is still being discussed in the literature [32], the reason for the absence of vibrational signals over Al_2O_3 requires further theoretical investigation beyond the scope of the present work.

The MgP molecules are adsorbed on an inhomogeneous Al_2O_3 layer grown on NiAl(110). The asymmetry of the multiple lobes in the rotational image of Fig. 3.3(e) is due to the non-uniform coupling of MgP to the inhomogeneous substrate, resulting in a non-planar geometry for the MgP and hence asymmetric interaction with the hydrogen. The asymmetry is not due to tip effect or lack of quality of the image and is a real effect. We used different tip-substrate distance and the image shown in Fig. 3.3(e) has the best quality corresponding to the optimized tip-substrate distance. The inhomogeneous Al_2O_3 surface also causes variations in the adsorption geometry and stability of different molecules, leading to the observed changes in the relative intensity of the lobes in the rotational image for different molecules.

The interaction between trapped H_2 and MgP is also sensitive to the distance between two molecules. The precise control of STM tip position allows us to modify the intermolecular distance by changing the tip-substrate separation. The IETS measurement of trapped H_2 over MgP and

FIG. 3.5. IETS measurements of trapped H_2 at different tip-substrate separations over MgP (a) and MgP^- (b). The bottom spectra are taken at $V_B = 50$ mV and $I_T = 0.1$ nA. The change in tip-substrate separation (Δz) is converted from the exponential dependence of the potential barrier height and the tunneling current. The spectra in (a) are the result of an average of 10 scans. The middle and bottom spectra in (b) are the result of an average of 50 scans, while the top spectrum is from a single scan. (c-d) Rotational d^2I/dV^2 images taken over two different MgP molecules at the same set point as Fig. 3.3(e). Multiple lobes are resolved but the molecules are less stable and switched during the scan. (e) Rotational d^2I/dV^2 image taken over the same MgP as for Fig. 3.3(e) at 43 mV, with a larger tip-substrate gap set by $V_B = 100$ mV and $I_T = 0.1$ nA, hence the inferior quality of the image.

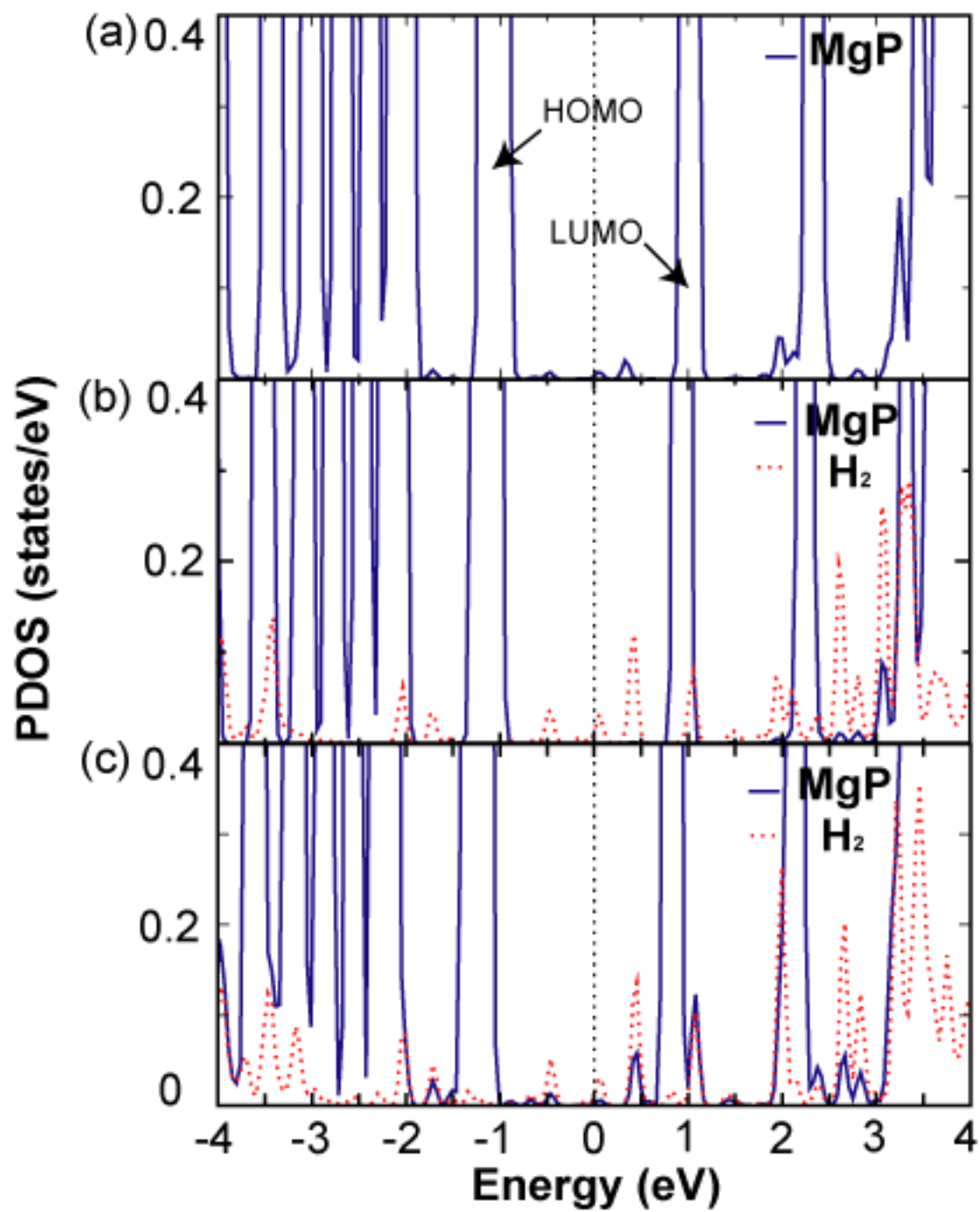


MgP⁻ at different tip-substrate separations are shown in Fig. 3.5. When the tip-substrate separation increases from $V_B = 50$ mV and $I_T = 0.1$ nA set point by 0.3 \AA , the H₂ rotational excitation energy shifts from 42 meV to around 45 meV over MgP. However, the change in spectra features over MgP⁻ is less obvious when the tip-substrate separation is changed by the same amount. The changes of rotational spectra with tip-substrate separation provide another indication that H₂-MgP interaction is stronger than H₂-MgP⁻ interaction. If the tip-substrate separation increases by 0.6 \AA , both the spectra over MgP or MgP⁻ become structureless, possibly due to the low probability of trapping a hydrogen molecule in the tip-substrate gap when the separation is large. Faint multiple lobes in the rotational image over MgP start to appear at $V_B = 100$ mV and $I_T = 0.1$ nA set point [Fig. 3.5(e)], and become more prominent when the tip-substrate distance decreases [Fig. 3.5(c-d), Fig. 3.3(e)]. However, the molecules become unstable as the tip-substrate distance continues to decrease, thus limiting spectromicroscopic measurements.

The calculated partial density of states at different tip-substrate separations are presented in Fig. 3.6. The presence of H₂ in the junction also shifts the Fermi level of MgP towards its LUMO at 6 \AA tip-substrate distance compared to the H₂-free junction at 4.5 \AA tip-substrate distance, demonstrating the change in electrostatic level is due to the MgP-H₂ interaction instead of MgP-tip interaction. A larger shift is observed when MgP is interacting with H₂ in a 4.5 \AA separation junction. This further demonstrates that the interaction mainly depends on the distance between MgP and H₂, and the hybridization with STM tip is not important.

We also study the interaction between H₂ and a single Au atom, another electron acceptor, to further validate H₂ as an electron donor. Electron transfer to a single Au atom to form Au⁻ has been shown to occur on the surface of NaCl film grown on Cu(100) [33]. The IETS measurement over NiAl(110) shows strong vibrational excitation signal at 15.2 mV for the H₂-surface bouncing

FIG. 3.6. Calculated partial density of states under different conditions for the tip-MgP junction (a) and tip-H₂-MgP junction (b-c). The distance between tip and MgP is set at 4.5 Å for (a) and (c), and 6 Å for (b). The Fermi level is indicated by the black dashed line. The H₂ molecule follows the configuration (5-d) in TABLE 3.1.

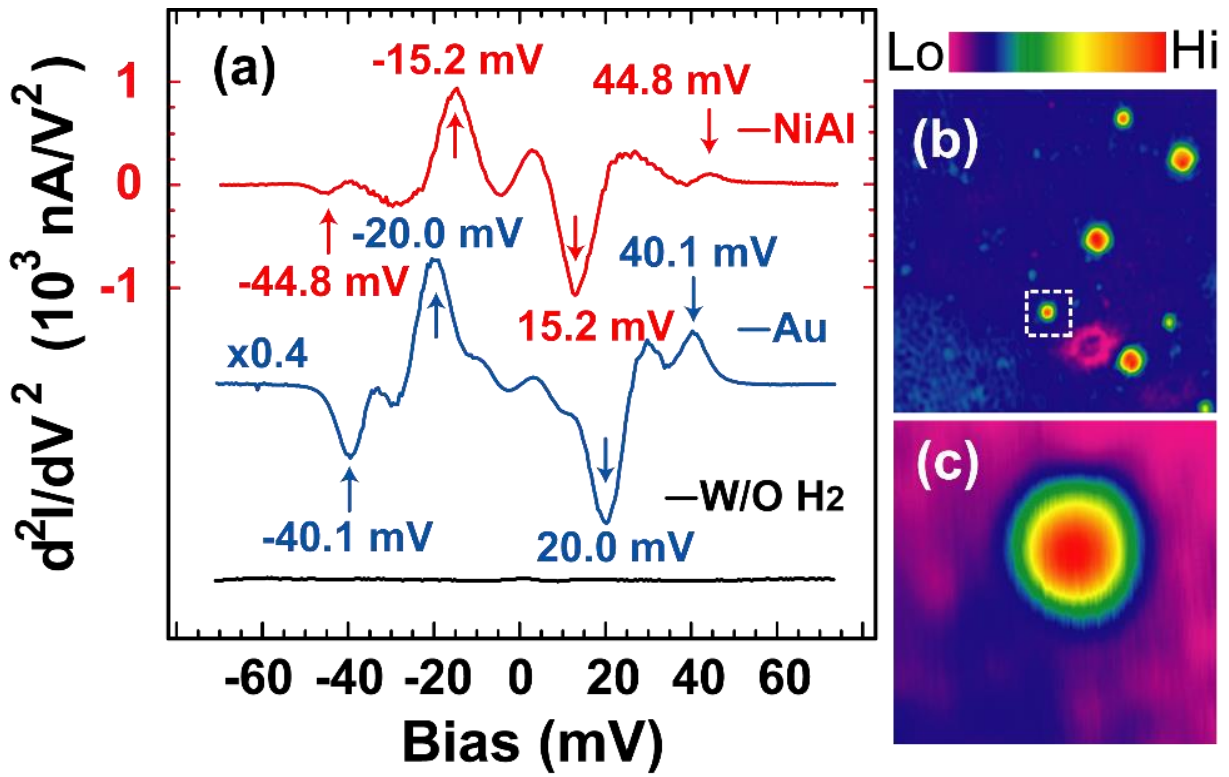


mode and a relatively weaker rotational feature at 44.8 mV [Fig. 3.7]. When the tip is located over an Au atom adsorbed on NiAl(110), the rotational excitation energy decreases to 40.1 meV and the vibrational excitation energy increase to 20.0 meV [Fig. 3.7(a)]. The increase in the vibrational energy coupled to the decrease in the rotational energy suggests a strengthened H-metal bond and a weakened H-H bond when the tip is positioned over the Au adatom [14]. These results strengthen the conclusion that the H₂ molecule acts as an electron donor and favorably interacts with an electron acceptor.

3.5 Conclusions

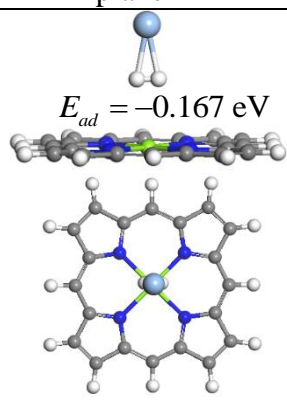
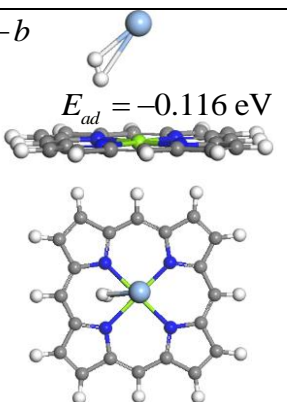
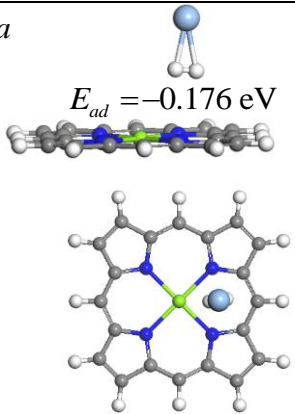
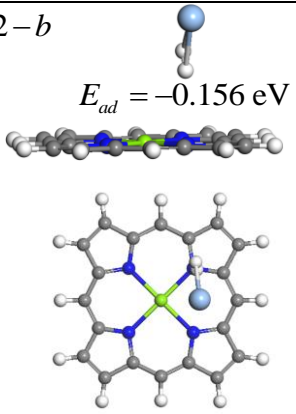
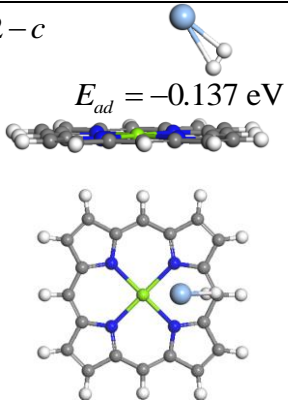
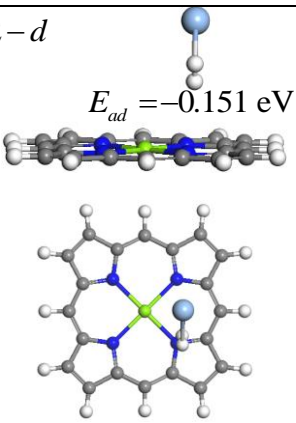
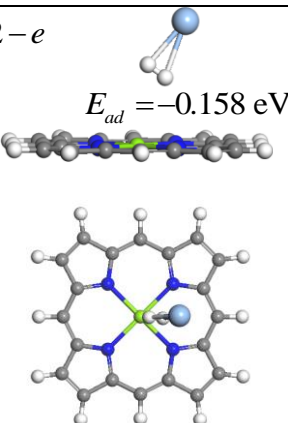
In summary, hydrogen rotational spectromicroscopy provides a novel approach toward visualizing and quantifying the intermolecular interaction between H₂ over another adsorbed molecule. The ability of the tip to trap a hydrogen molecule as it scans over another adsorbed molecule combined with the sensitivity of the hydrogen rotational excitation recorded by IETS to its immediate environment lead to the implementation of rotational spectromicroscopy. Here we apply this new probe to image the interaction between a hydrogen molecule on top of (instead of next to) a MgP on Al₂O₃ surface. The similarity between the hydrogen rotational image and the LUMO image of MgP suggests that hydrogen orbitals interact with the LUMO of MgP. This conclusion is based on the expectation that the rotational intensity tracks the preferable location of the freely rotating hydrogen over the molecule, and the shift in the rotational energy reflects the change in H-H bond strength. In contrast, the coupling is not favored between hydrogen and the SUMO of anionic MgP⁻. The electron transfer from $\sigma_{\text{H-H}}$ to the empty LUMO in the neutral MgP is critical in this donor-acceptor interaction. The σ -donor nature of H₂ is further confirmed by DFT calculations as well as its interaction with an electronegative Au atom adsorbed on the NiAl(110)

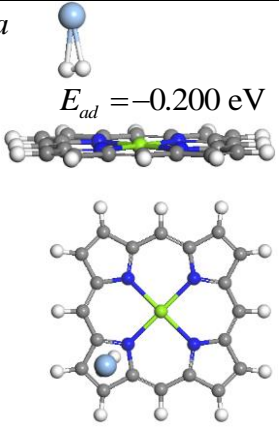
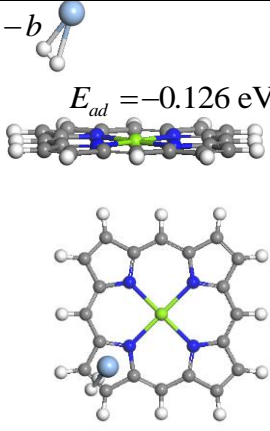
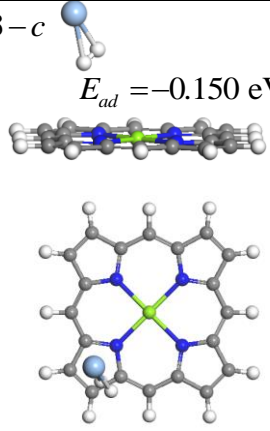
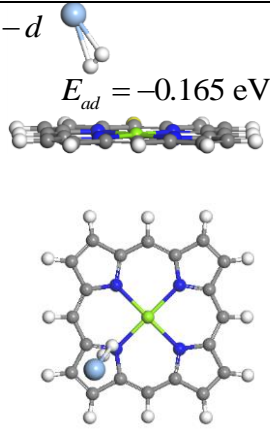
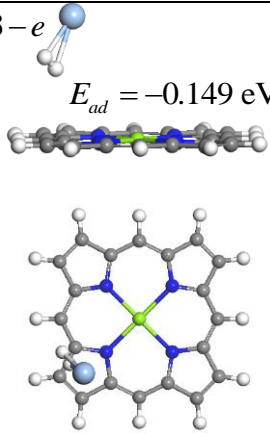
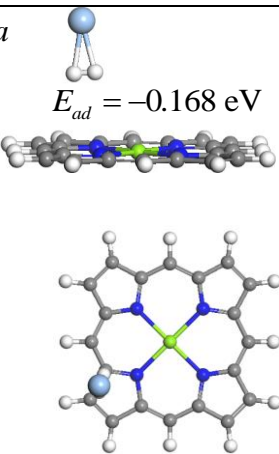
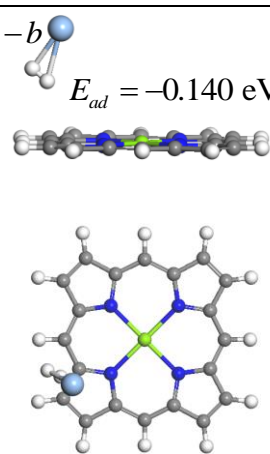
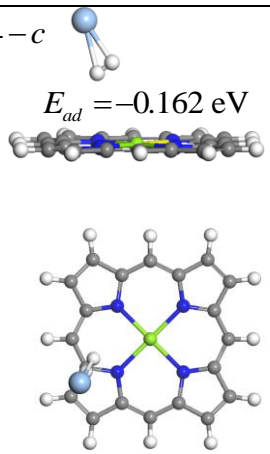
FIG. 3.7. Spectral shifts over an Au adatom. (a) d^2I/dV^2 spectra of H_2 trapped over NiAl(110) substrate (top spectrum) and an Au adatom (middle spectrum). The $j=0 \rightarrow 2$ rotational excitation energy of H_2 is 44.8 meV over NiAl(110) substrate and 40.1 meV over Au adatom. The $v=0 \rightarrow 1$ vibrational excitation energy of the H_2 -surface bouncing mode is 15.2 meV over NiAl(110) substrate and 20.0 meV over Au adatom. The d^2I/dV^2 spectra (BK) taken before dosing H_2 and over NiAl (bottom spectrum) is nearly featureless. All the spectra are taken with set point $V_B = 50$ mV, $I_T = 1$ nA. (b) Topographic image of Au adatoms on NiAl(110); Au adatom (marked by dotted box) appears as a small round protrusion. The larger square protrusions are adsorbed MgP molecules. (c) Zoom in topographic image of the Au adatom marked in (b). The set point is $V_B = 100$ mV, $I_T = 0.1$ nA for both (b) and (c).



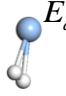

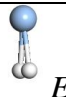
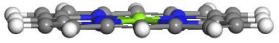
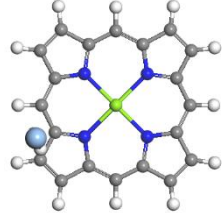
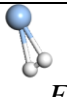

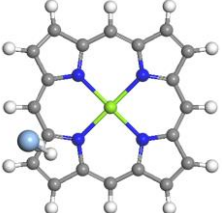
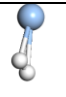

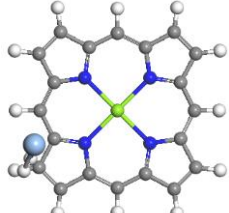


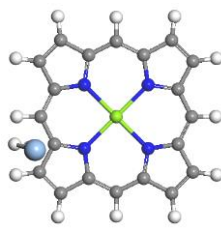


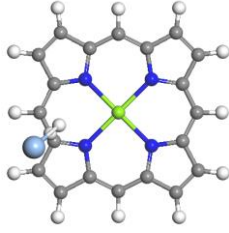


surface. The rotational spectromicroscopy extends the study of intermolecular interactions in the direction perpendicular to the surface.

TABLE 3.1. DFT results of H₂ adsorption energies at different positions over MgP as indicated in Fig. 3.4(b). The distance between tip and substrate is set at 4.5 Å.

	H-H parallel to the MgP plane	H-H tilted from the MgP plane	
Tip at position 1	<p>1-a</p>  <p>$E_{ad} = -0.167 \text{ eV}$</p>	<p>1-b</p>  <p>$E_{ad} = -0.116 \text{ eV}$</p>	
Tip at position 2	<p>2-a</p>  <p>$E_{ad} = -0.176 \text{ eV}$</p>	<p>2-b</p>  <p>$E_{ad} = -0.156 \text{ eV}$</p>	<p>2-c</p>  <p>$E_{ad} = -0.137 \text{ eV}$</p>
		<p>2-d</p>  <p>$E_{ad} = -0.151 \text{ eV}$</p>	<p>2-e</p>  <p>$E_{ad} = -0.158 \text{ eV}$</p>

<p>Tip at position 3</p>	<p>3-a</p>  <p>$E_{ad} = -0.200$ eV</p>	<p>3-b</p>  <p>$E_{ad} = -0.126$ eV</p>	<p>3-c</p>  <p>$E_{ad} = -0.150$ eV</p>
		<p>3-d</p>  <p>$E_{ad} = -0.165$ eV</p>	<p>3-e</p>  <p>$E_{ad} = -0.149$ eV</p>
<p>Tip at position 4</p>	<p>4-a</p>  <p>$E_{ad} = -0.168$ eV</p>	<p>4-b</p>  <p>$E_{ad} = -0.140$ eV</p>	<p>4-c</p>  <p>$E_{ad} = -0.162$ eV</p>

		<p>4-d</p> <p>$E_{ad} = -0.181 \text{ eV}$</p>  	<p>4-e</p> <p>$E_{ad} = -0.125 \text{ eV}$</p>  
Tip at position 5	<p>5-a</p> <p>$E_{ad} = -0.143 \text{ eV}$</p>   	<p>5-b</p> <p>$E_{ad} = -0.156 \text{ eV}$</p>   	<p>5-c</p> <p>$E_{ad} = -0.129 \text{ eV}$</p>   
		<p>5-d</p> <p>$E_{ad} = -0.148 \text{ eV}$</p>   	<p>5-e</p> <p>$E_{ad} = -0.148 \text{ eV}$</p>   

3.6 Bibliography

- [1] S. L. Cockroft and C. A. Hunter, *Chem. Soc. Rev.* **36**, 172 (2007).
- [2] J. K. Gimzewski and C. Joachim, *Science* **283**, 1683 (1999).
- [3] A. E. Reed, L. A. Curtiss, and F. Weinhold, *Chem. Rev.* **88**, 899 (1988).
- [4] H. J. Lee and W. Ho, *Science* **26**, 1719 (1999).
- [5] Y. Jiang, Q. Huan, L. Fabris, G. C. Bazan, and W. Ho, *Nature Chem.* **5**, 36 (2013).
- [6] J. Zhang, P. Chen, B. Yuan, W. Ji, Z. Cheng, and X. Qiu, *Science* **342**, 611 (2013).
- [7] C. Weiss, C. Wagner, R. Temirov, and F. S. Tautz, *J. Am. Chem. Soc.* **132**, 11864 (2010).
- [8] C. Chiang, C. Xu, Z. Han, and W. Ho, *Science* **344**, 885 (2014).
- [9] C. A. Hunter, *Angew. Chem. Int. Ed.* **43**, 5310 (2004).
- [10] S. W. Wu, N. Ogawa, and W. Ho, *Science* **312**, 1362 (2006).
- [11] S. W. Wu, N. Ogawa, G. V. Nazin, and W. Ho, *J. Phys. Chem. C*, **112**, 5241 (2008).
- [12] W. L. Yim, J. S. Tse, and T. Iitaka, *Phys. Rev. Lett.* **105**, 215501 (2010).
- [13] C. S. Carr and J. B. Hughes, *Environ. Sci. Technol.*, **32**, 1817 (1998).
- [14] S. Li, A. Yu, F. Toledo, Z. Han, H. Wang, H. Y. He, R. Wu, and W. Ho, *Phys. Rev. Lett.* **111**, 146102 (2013).
- [15] J. A. Gupta, C. P. Lutz, A. J. Heinrich, and D. M. Eigler, *Phys. Rev. B* **71**, 115416 (2005).
- [16] C. Weiss, C. Wagner, C. Kleimann, M. Rohlfing, F. S. Tautz, and R. Temirov, *Phys. Rev. Lett.* **105**, 086103 (2010).
- [17] G. Kichin, C. Wagner, F. S. Tautz, and R. Temirov, *Phys. Rev. B* **87**, 081408 (2013).
- [18] B. C. Stipe, M. A. Rezaei, and W. Ho, *Rev. Sci. Instrum.* **70**, 137, (1999).
- [19] X. H. Qiu, G. V. Nazin, and W. Ho, *Science* **299**, 542, (2003).
- [20] G. Kresse and J. Hafner, *Phys. Rev. B* **47**, 558 (1993).

- [21] G. Kresse and J. Hafner, Phys. Rev. B **49**, 14251 (1994).
- [22] G. Kresse and J. Furthmuller, Phys. Rev. B **54**, 11169 (1996).
- [23] P. E. Blochl, Phys. Rev. B **50**, 17953 (1994).
- [24] J. Klimeš, D. R. Bowler, and A. Michaelides, Phys. Rev. B **83**, 195131 (2011).
- [25] J. Klimeš, D. R. Bowler, and A. Michaelides, J. Phys.: Cond. Matt. **22**, 022201 (2010).
- [26] H. J. Monkhorst and J. D. Pack, Phys. Rev. B **13**, 5188 (1976).
- [27] J. B. Maddox, U. Harbola, K. Mayoral, and S. J. Mukamel, Phys. Chem. C **111**, 9516 (2007).
- [28] F. D. Natterer, F. Patthey, and H. Brune, Phys. Rev. Lett. **111**, 175303 (2013).
- [29] N. Lorente and M. Persson, Phys. Rev. Lett. **85**, 2997 (2000).
- [30] F. D. Natterer, F. Patthey, and H. Brune, ACS Nano **8**, 7099 (2014).
- [31] G. J. Kubas, Proc. Natl. Acad. Sci. U.S.A. **104**, 6901 (2007).
- [32] N. Lorente, M. Persson, L. J. Lauhon, and W. Ho, Phys. Rev. Lett. **86**, 2593 (2001).
- [33] J. Repp, G. Meyer, F.E. Olsson, and M. Persson, Science **305**, 493 (2004).

Chapter 4

Conclusions and Prospects

4.1 Concluding Remarks

In conclusion, the results presented in this thesis demonstrate the possibility of detecting the rotational excitations of a single molecule on surfaces using the STM. The rotational motion of a single molecule can be very sensitive to its local chemical environment and can be used as a probe to characterize the intermolecular interactions. In Chapter 2, we presented the measurement of $j=0$ to $j=2$ rotational excitations of H_2 , D_2 , and HD on $Au(110)$ surface. The rotational energies can change with the tip-substrate distance, which indicates a weakened H-H bond when the H_2 couples strongly to the metal tip and substrate. In Chapter 3, we further took use of the sensitivity of H_2 rotational excitation to characterize its interaction with MgP, MgP- and Au atom. The H_2 rotational images reveal that H_2 interacts strongly with MgP LUMO, but not MgP- SUMO. These results shown the electron donor nature of H_2 which is also confirmed by its interaction to the electronegative Au atoms. The single molecule rotational spectroscopy and microscopy provide novel approaches towards probing the chemical structure and interactions with ultra-high spatial resolution.

4.2 Prospects for the Future

The experiments in this thesis show that the rotational spectroscopy and microscopy can both be powerful surface analytical techniques. It is possible to use the rotational excitation energy to probe the structural change of a molecule during a chemical reaction. For example, as shown in

Chapter 2, the decrease of tip-substrate separation will weaken the H-H bond. As the junction keeps shrinking, the H-H bond may break and H atoms can form new bonds with the metal surfaces or molecules underneath [1, 2]. The rotational spectroscopy may be used to visualize the spatial variation in the reaction processes and the activation energies.

The unconventional line shape of the rotational STM-IETS also requires combined experimental and theoretical studies. Traditionally, STM-IETS show peaks at the positive bias side in the d^2I/dV^2 spectra as stated in the Chapter 1. Sometime a dip or a Fano line shape (peak with a side dip) can be observed [3], which can be explained by the coupling between inelastic electron tunneling channel and elastic electron tunneling channel [4]. In rotational STM-IETS of H₂, the line shapes are often found to be Fano line shape. The line shapes varied a lot between MgP and MgP-. The origin of the variations requires further investigations.

Moreover, rotational STM-IETS can be a unique technique to investigate H₂ ortho-para transition in real space. At room temperature, ratio of ortho-H₂ and para-H₂ should be 3:1 due to the thermal excitation. The natural ortho-para transition rate should be low without catalysis at low temperature [5]. However, the ortho-H₂ can rapidly relax into the para state when adsorbed on noble metal surfaces at low temperature. The origin of this fast ortho-para transition is still under debate [6]. The real space rotational spectroscopy and microscopy could monitor both the temporal and spatial variations of the ortho-hydrogen, which is crucial to reveal the nature of this phenomena.

4.4 Bibliography

[1] J. Harris, *Langmuir* **7**, 2528 (1991).

[2] J. A. White, D. M. Bird, *Phys. Rev. Lett.* **73**, 1404 (1994).

- [3] W. Ho, J. Chem. Phys. **117**, 11033 (2002).
- [4] N. Lorente and M. Persson, Phys. Rev. Lett. **85**, 2997 (2000).
- [5] E. Ilisca, Phys Rev Lett. 66, 667 (1991).
- [6] I. F. Silvera, Rev. Mod. Phys. **52**, 393 (1980).